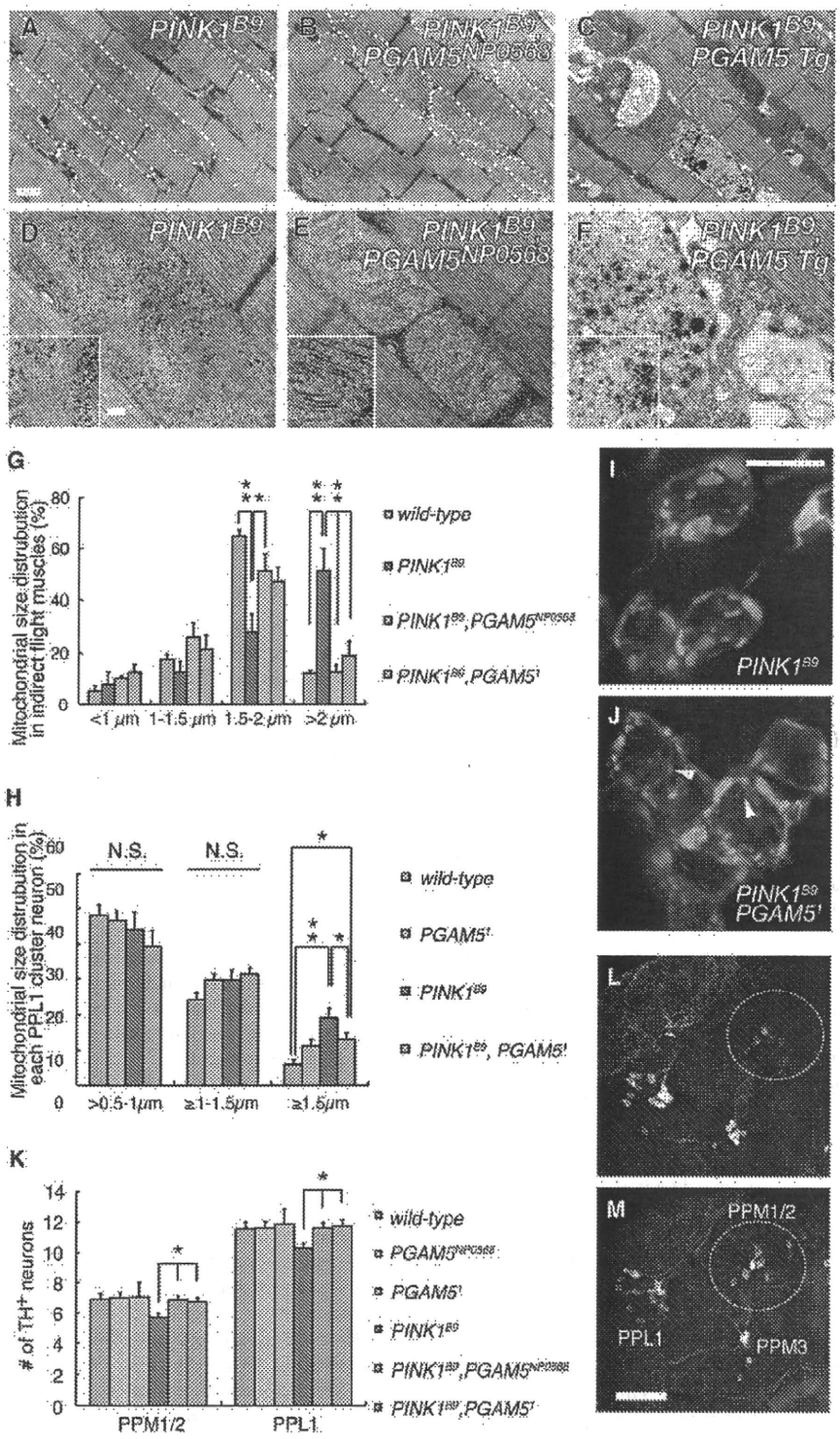

Figure 6. Loss of *dPGAM5* improves degeneration of the mitochondria and DA neurons caused by *dPINK1* inactivation in *Drosophila*. (A–F) TEM analysis of the indirect flight muscle and morphology of mitochondria in 2-day-old adult flies with the indicated genotypes. In A and B, some mitochondria are outlined with broken lines. The insets in D–F show representative mitochondria matrixes. Scale bars = 1 μm in A–C and 200 nm in D–F. (G) Quantification of the percentage of mitochondrial size distribution in the indirect muscle tissue from *wild-type* ($n = 136$ from 5 adult flies), *PINK1*^{B9} ($n = 96$ from 5), *PINK1*^{B9}, *PGAM5*^{NP0568} ($n = 116$ from 5), *PINK1*^{B9}, *PGAM5*^{1} ($n = 111$ from 5) as shown in Figure 3K. Data are shown as means ± SE (* $p<0.05$, ** $p<0.01$). (H–J) Quantification of the percentage of cytoplasmic mitochondrial aggregates with diameter of 0.5–1.0, 1.0–1.5 or ≥1.5 μm in each PPL1 TH^{+} neuron from *wild-type* ($n = 373$ from 18 adult flies), *PGAM5*^{1} ($n = 356$ from 18), *PINK1*^{B9} ($n = 231$ from 11), *PINK1*^{B9}*PGAM5*^{1}

flies ($n=235$ from 13). Mitochondrial morphology was revealed by mitoGFP as shown in Figure 3L–3O. Data are shown as means ± SE (*, $p<0.05$; **, $p<0.01$; N.S., not significant). Tubular or reticular mitochondria were excluded from the estimation due to difficulty in the counting. However, the ratio of mitochondria with that morphology was also increased in *PINK1*^{B9}*PGAM5*^{1} flies (J) compared with that in *PINK1*^{B9} flies (I). Arrowheads in (J) indicate representative tubular or reticular mitochondria. Scale bar in (I) = 5 μm. (K) Quantification of TH^{+} DA neuron number in the PPM1, PPM2 and PPL1 clusters in 25-day-old males. PPM1 and PPM2 cluster neurons were counted together. Data are shown as means ± SE (*, $p<0.05$; $n=16$). (L, M) Representative images of PPM1/2, PPM3 and PPL1 clusters of *PINK1*^{B9} (L) and *PINK1*^{B9}, *PGAM5*^{NP0568} flies (M) visualized with anti-TH antibody. Scale bar in (M) =50 μm. The genotypes are: *PINK1*^{RV}/*Y* (*wild-type*), *PINK1*^{B9}/*Y* (*PINK1*^{B9}), *PGAM5*^{NP0568}/*Y* (*PGAM5*^{NP0568}), *PGAM5*^{1}/*Y* (*PGAM5*^{1}), *PINK1*^{B9}, *PGAM5*^{NP0568}/*Y* (*PINK1*^{B9}, *PGAM5*^{NP0568}), *PINK1*^{B9}, *PGAM5*^{1}/*Y* (*PINK1*^{B9}, *PGAM5*^{1}), *PINK1*^{B9}/*Y*; *Da-GAL4*> *dPGAM5* (*PINK1*^{B9}, *PGAM5 Tg*), in (A–G, K–M), *PINK1*^{RV}/*Y*; *TH-GAL4*> *mitoGFP* (*wild-type*), *PINK1*^{B9}/*Y*; *TH-GAL4*> *mitoGFP* (*PINK1*^{B9}), *PGAM5*^{1}/*Y*; *TH-GAL4*> *mitoGFP* (*PGAM5*^{1}), *PINK1*^{B9}, *PGAM5*^{1}/*Y*; *TH-GAL4*> *mitoGFP* (*PINK1*^{B9}, *PGAM5*^{1}) in (H–J).

doi:10.1371/journal.pgen.1001229.g006

known mitochondrial fusion/fission machinery suggested that PGAM5 acts upstream of them or in an independent pathway (Figure 4). Given that PGAM5 is involved in mitochondrial fission, loss of PGAM5 would be expected to enhance the *PINK1* mutant phenotype in *Drosophila*, similar to the interaction between *PINK1* and the mitochondrial fusion/fission machinery [10–12]. Interestingly, the number of large aggregated mitochondria, which are frequently seen in *PINK1*^{B9} flies, was mildly decreased in TH^{+} neurons of *PINK1*^{B9}*PGAM5*^{1} flies (Figure 6H–6J). Moreover, loss of dPGAM5 also modulated the mitochondrial morphology of *dParkin* mutant fly without suppressing the mitochondrial degeneration (Figure 7H–7L). Based on these observations, it could be speculated that PGAM5 does not directly regulate mitochondrial fission but instead, modulates the PINK1 pathway in a different way. Recent studies have proposed two different models for the mechanism of mitochondrial morphological changes through the PINK1/Parkin pathway in *Drosophila* and mammals. Ziviani *et al.* and Poole *et al.* have demonstrated that dParkin promotes degradation of Mfn in a dPINK1-dependent manner, which leads to mitochondrial fragmentation in *Drosophila* [16,36]. Our current results demonstrated that the loss of dPGAM5 activity does not affect mitochondrial fragmentation caused by reduction of Mfn activity, suggesting that dPGAM5 might not contribute to the proposed PINK1/Parkin pathway (Figure 4). Sandebring *et al.* have proposed that accumulation of damaged mitochondria by PINK1 inactivation results in mitochondrial calcium efflux, which activates Drp1 through Calcineurin-mediated dephosphorylation of Drp1 in human cells [37]. This model well explains the observation that loss of PINK1 indirectly promotes mitochondrial fragmentation in mammalian cells and the indication that PINK1 is not a core component of the fusion/fission machinery in a *Drosophila* study [11]. However, most of *Drosophila* studies do not support a result that loss of PINK1 leads to mitochondrial fragmentation in mammals. Thus, it still remains a question for further investigation how PGAM5 modulates the mitochondrial dynamics.

Although the property of PGAM5 to physically interact with PINK1 appears to be conserved between human and *Drosophila*, the functional significance of this binding remains to be established. PINK1 and PGAM5 have kinase and phosphatase activities, respectively. However, there is no evidence to suggest that PINK1 directly phosphorylates PGAM5, or that PGAM5 dephosphorylates PINK1 (Figure 2G and 2H) [18,25,26]. The PINK1 protein levels are maintained at very low level under steady-state conditions by constitutive processing and subsequent degradation through the ubiquitin-proteasome pathway [15]. Recent studies suggested that PINK1 selectively translocates from cytosol to mitochondria with low membrane potential, at which PINK1 is stabilized [14,15,38]. The accumulated PINK1 on the depolarized mitochondria further recruits Parkin to induce mitophagy [13–15,38]. However, Parkin does not seem to be the target of PINK1 kinase activity [15], and PINK1 does not seem to activate Parkin E3 activity directly (data not shown). Based on these findings, it is possible that PGAM5 may promote a selective recruitment of PINK1 to the outer membrane of the damaged mitochondria, or that PGAM5 may regulate PINK1 stabilization. Our molecular analysis, however, did not support the idea that PGAM5 stabilizes PINK1 (data not shown). In addition, because loss of *dPGAM5* partially suppresses *dPINK1* null phenotypes, it seems likely that PINK1 negatively regulates PGAM5 function (Figure 9). PGAM5 was originally identified as a Bcl-xL-binding protein, and in itself can be toxic to cells, promoting mitochondrial fragmentation, when expressed at high levels (Figure 3B). Therefore, it seems possible that PGAM5 modulates a cell protective or a mitochondrial morphogenetic activity of the Bcl-2 family member Bcl-xL downstream of PINK1 but in a pathway that is independent from Parkin (Figure 9A) [39]. In this context, PINK1 may suppress the cell toxic action of PGAM5 through an indirect mechanism where an unidentified substrate of PINK1 inactivates PGAM5. Interestingly, a recent report suggests that the *dPINK1* phenotype can be partially suppressed by transgenic expression of *Drosophila* Bcl-2 protein Buffy [8]. Alternatively, PGAM5 may be one of components of a negative regulator complex against Parkin E3, downstream of PINK1 (Figure 9B). Matsuda *et al.* have reported that Parkin E3 activity is activated only at the depolarized mitochondria, suggesting the existence of its negative regulator(s) [38]. E3 activity of Parkin may be released when PINK1 associates with the negative regulator complex via PGAM5 and suppresses its function by phosphorylation of another complex component(s). This idea might be partly supported by our observation that loss of *dPGAM5* had little effect on *dparkin* mutant flies.

Although the primary cause of the mitochondrial degeneration by the loss of *PINK1* remains less obvious, the growing evidence suggests that PINK1 eliminates oxidatively damaged mitochondria in cooperation with Parkin, the failure of which leads to tissue degeneration. Supporting for this hypothesis, the mitochondrial phenotypes of *dPINK1* and *dParkin* mutant flies are primarily exhibited in similar tissues that require higher energy demands [7–9]. Although dPAGM5 might not regulate Keap1 function in *Drosophila*, the Keap1/Nrf2 pathway appears to be conserved in *Drosophila* [32], and activation of the Keap1/Nrf2 pathway by genetic manipulation effectively suppressed the short-lifespan phenotype by *dPINK1* inactivation. This finding may also support the above idea that the accumulation of oxidatively damaged mitochondria leads to degeneration of specific tissues, providing a hint of therapeutic strategies for *PINK1*-associated PD.

In conclusion, the results of our genetic study demonstrate that the mitochondrial-localized protein PGAM5 modulates the PINK1 pathway in *Drosophila*. However, further work will be required to determine how PGAM5 regulates the PINK1 pathway at the molecular level, as well as to determine if manipulation of PGAM5 activity might provide a therapeutic advantage in treatment of *PINK1*-associated PD.

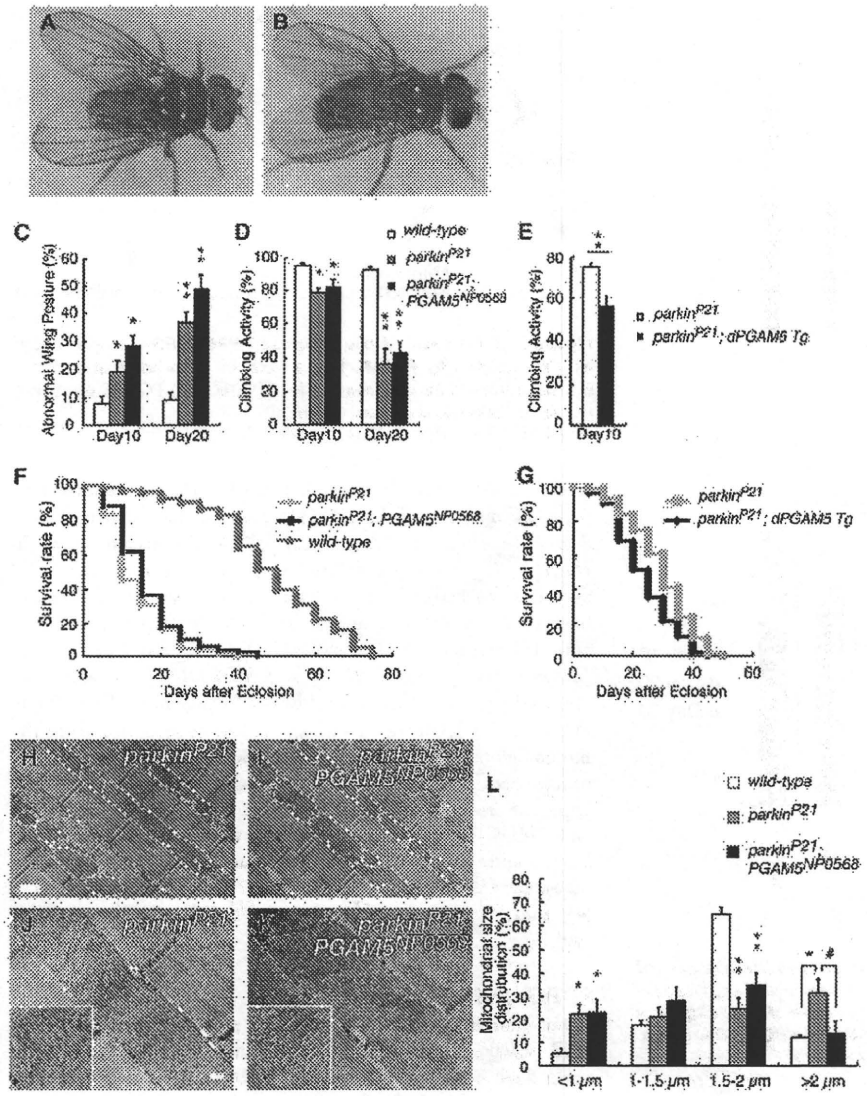

Figure 7. Disruption of *dPGAM5* fails to suppress the mitochondrial phenotype caused by *dParkin* inactivation in *Drosophila*. The abnormal wing posture caused by a homozygous *dParkin* mutation (A) was not suppressed by removal of the *dPGAM5* gene (B). (C) Percentage of flies with abnormal wing posture among 10- and 20-day-old male *wild-type* ($n=105$), $parkin^{P21}$ ($n=102$) and $PGAM5^{NP0568}$; $parkin^{P21}$ ($n=109$) flies. Error bars show S.E. from three repeated experiments. *, $p<0.05$; **, $p<0.01$ *vs. dParkin*(+/+). (D) Percentage of flies showing locomotor activity among 10- and 20-day-old male $parkin^{P21}$ ($n=86$), $parkin^{P21}$ ($n=73$) and $PGAM5^{NP0568}$; $parkin^{P21}$ ($n=78$) flies. Error bars show S.E. from twenty repeated experiments. *, $p<0.05$; **, $p<0.01$ *vs. dParkin*(+/+). (E) Locomotor activity of 10-day-old male $parkin^{P21}$ ($n=153$) and $parkin^{P21}$ ubiquitously overexpressing *dPGAM5* flies ($parkin^{P21}$; *dPGAM5 Tg*, $n=155$) flies. Error bars show S.E. from twenty repeated experiments. **, $p<0.01$. (F) Lifespan of adult male *wild-type* ($n=104$), $parkin^{P21}$ ($n=102$) and $PGAM5^{NP0568}$; $parkin^{P21}$ ($n=91$) flies. $PGAM5^{NP0568}$; $parkin^{P21}$ *vs.* $parkin^{P21}$, $p=0.191$; *wild-type vs.* $parkin^{P21}$, $p<0.001$ by log rank test. (G) Lifespan of adult male $parkin^{P21}$ ($n=153$) and $parkin^{P21}$; *dPGAM5 Tg* flies ($n=155$) flies. $parkin^{P21}$ *vs.* $parkin^{P21}$; *dPGAM5 Tg*, $p<0.001$ by log rank test. (H–K) TEM analysis of the indirect flight muscle and mitochondrial morphology in tissue from flies of the indicated genotypes. The long tubular mitochondrial phenotype seen in $parkin^{P21}$ flies can be rescued by *dPGAM5* inactivation (H and I). However, the mitochondrial matrix still appears degenerated (insets in J and K). Scale bars = 1 μm in H and I and 200 nm in J and K. (L) Quantification of the percentage of mitochondrial size distribution in the indirect muscle tissue from *wild-type* ($n=136$ from 5 adult flies), $parkin^{P21}$ ($n=89$ from 5) and $parkin^{P21}$; $PGAM5^{NP0568}$ flies ($n=84$ from 5) as shown in (H–K). The length of the mitochondria in the direction of the myofibrils was measured. Data are shown as means ± SE (* $p<0.05$, ** $p<0.01$ *vs. wild-type*; # $p<0.05$ *vs.* $parkin^{P21}$; $PGAM5^{NP0568}$). The genotypes are: +/Y (*wild-type*), +/Y; $parkin^{P21}$/$parkin^{P21}$ ($parkin^{P21}$), $PGAM5^{NP0568}$/Y; $parkin^{P21}$/$parkin^{P21}$ ($parkin^{P21}$; $PGAM5^{NP0568}$).
doi:10.1371/journal.pgen.1001229.g007

Materials and Methods

Purification of PINK1-Binding Proteins

HEK293 cells stably expressing hPINK1-FLAG or parent cells were grown in suspension culture (Joklik-modified Eagle's minimum essential medium with 5% fetal bovine serum). The cell pellet (2.4×10^8 cells) was homogenized in lysis buffer (50 mM Tris pH 7.4, 120 mM NaCl, 5 mM EDTA, 10% glycerol, 1% Trion-X100) supplemented with Complete Protease Inhibitors (Roche Diagnostics). The soluble fraction of the suspension was

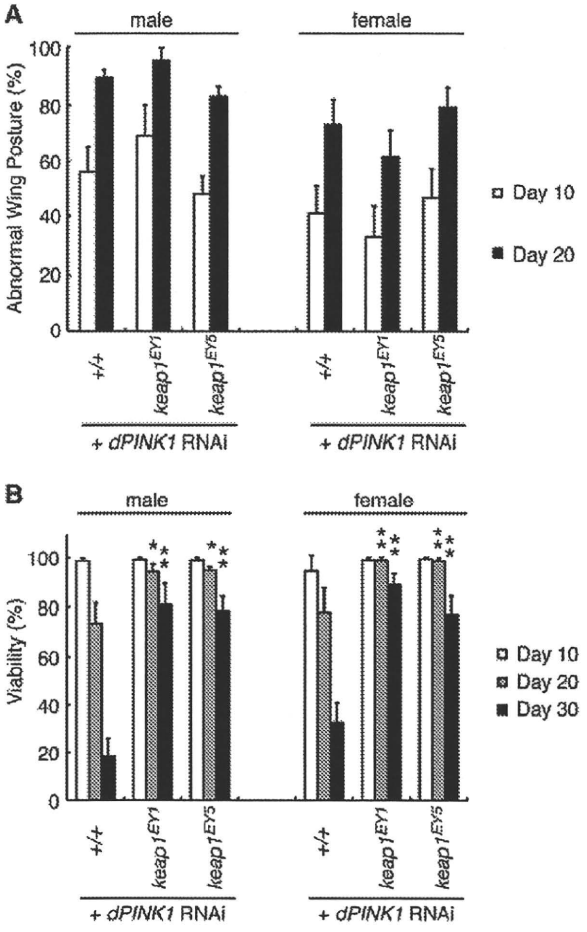

Figure 8. Reduction of Keap1 activity improves the lifespan of *dPINK1* RNAi flies. Removal of one copy of *Drosophila keap1* had no effects on the wing phenotype of *dPINK1* RNAi flies (A) but improved viability (B). *, $p<0.05$; **, $p<0.01$ *vs.* age-matched *dPINK1* RNAi group. The genotypes are as follows: *MHC-GAL4> dPINK1^{RNAi}* (+/+), *MHC-GAL4> dPINK1^{RNAi}/Keap^{EY1}* (*Keap^{EY1}*), *MHC-GAL4> dPINK1^{RNAi}/Keap^{EY5}* (*Keap^{EY5}*). Flies were raised at 29°C.
doi:10.1371/journal.pgen.1001229.g008

immunoprecipitated with anti-FLAG M2 agarose (Sigma-Aldrich) and washed five times in lysis buffer. The fractions eluted with 200 μg/ml 3x FLAG peptide were resolved by SDS-PAGE. Specific bands detected by silver staining were excised for in-gel digestion. The digest extracted from the gel was subjected to online HPLC-MS/MS, followed by informatics-based identification of the proteins (Nippon Proteomics).

Drosophila Genetics

Fly culture and crosses were performed on standard fly food containing yeast, cornmeal and molasses, and flies were raised at 25°C unless otherwise indicated. To generate *UAS-dPGAM5* transgenic lines, cDNA for *dPGAM5* and *dPGAM5-2* obtained by RT-PCR from adult *Drosophila* total RNA was subcloned into the *pUAST* vector. Introduction of transgenes into *Drosophila* germ line and establishment of transgenic lines into a *w* background were performed by BestGene Inc. (Chino Hills, CA). A *P*-element insertion line for *dPGAM5* mutant, *PGAM5^{NP0568}* obtained from Kyoto *Drosophila* Genetic Resource Center, expresses a reduced

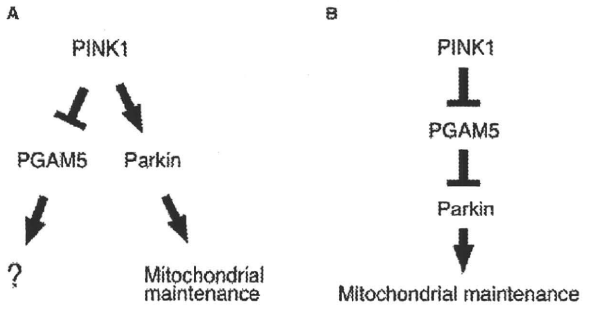

Figure 9. Schematic of the proposed PINK1/PGAM5 pathways in *Drosophila*. (A) PGAM5 has a role in mitochondrial activities independently of Parkin downstream of PINK1. (B) PGAM5 negatively regulates Parkin downstream of PINK1.
doi:10.1371/journal.pgen.1001229.g009

level (~25%) of mRNA, in which *NP0568* element is integrated 50 bp downstream of the *dPGAM5* translational start site (Figure S1B). We could not detect any dPGAM5 protein signal in *PGAM5^{NP0568}* homozygous flies (Figure S1C). The *PGAM5^{NP0568}* line was backcrossed to *w* for six generations to remove background mutations, and used for most experiments as a *dPGAM5* mutant line. *UAS-dPGAM5* RNAi (VDRC 51655) and *UAS-mfn* RNAi (VDRC105261 and VDRC40478) strains were obtained from the Vienna *Drosophila* RNAi Center. To generate *PGAM5^{1}*, the KG09727 *P*-element insertion (obtained from the Bloomington *Drosophila* Stock Center) was mobilized using *Δ2–3* transposase, and the entire dPGAM5 coding region was deleted by imprecise excision, as shown in Figure S1A. All other fly stocks and *GAL4* lines used in this study were obtained from the Bloomington *Drosophila* Stock Center and have been previously described: *UAS-dPINK1 RNAi* [9]; *PINK1^{B9}* and revertant *PINK1^{RV}* [8]; *parkin^{P21}* [30]; *keap1^{EY1}*and *keap1^{EY5}* [32]; *Drp1^{2}* and *Drp1^{+}* [40].

RT-PCR and Plasmids

For quantitative RT-PCR analysis, reverse transcription and PCR reactions with total RNA extracted from fly heads were performed using a Superscript VILO cDNA synthesis kit (Invitrogen) and SYBR GreenER qPCR SuperMix (Invitrogen), respectively. Full-length cDNAs corresponding to *hPGAM5* (GenBank NP_001170543) and a short isoform of *hPGAM5* (hPGAM5-S, GenBank NM_138575) were amplified by RT-PCR from total RNA purified from HEK293 cells or a cDNA clone (RIKEN clone ID: IRAK003D15), and was cloned in *pcDNA3-Myc*, *pGEX6P-1* and *pGEX4T-1* vectors. Expression plasmids for *hPINK1-FLAG* and *pUAST-dPINK1-Myc* have been reported elsewhere [9,20].

Antibodies

Rabbit anti-human PGAM5 polyclonal antibody was raised against recombinant GST-tagged PGAM5 domain (89–289 aa) produced in the *E. coli* strain BL21(DE3)pLysS (Novagen), and was affinity-purified against the antigen. Rabbit anti-dPGAM5 polyclonal antibody was raised against the peptide ELLTNRIPRDVKNVV. Anti-hPINK1 antibody (BC100-494), anti-Myc (4A6) and anti-FLAG (M2) antibodies were purchased from Novus, Millipore and Sigma-Aldrich, respectively. Mouse anti-TH monoclonal antibody was purchased from ImmunoStar, and rabbit anti-*Drosophila* TH polyclonal antibody was described previously [9].

Cell Culture, Immunoprecipitation, and Immunoblot Analysis

Transfection of mammalian cultured cell, immunopurification of FLAG-protein from transfected cell lysate and immunoblot analysis was performed as described previously [4,41]. For the hPGAM5 RNAi experiment, HEK293 cell lysate transfected with 20 μM stealth RNAi reagent against hPGAM5 or a control RNAi reagent (Invitrogen), was analyzed 72 hrs after transfection. To detect an endogenous interaction between PINK1 and PGAM5, we treated HEK293 cells (2×10^7 cells) with 20 μM carbonyl cyanide 3-chlorophenylhydrazone for 24 hrs to induce a sufficient level of human PINK1 protein for the study. The treated cells were subjected to immunoprecipitation using a Rabbit TrueBlot kit combined with rabbit anti-human PINK1 or rabbit anti-Delta (Santa Cruz) as a species-matched control. For the preparation of fly samples for immunoblot analysis, fly heads were directly homogenized in 20 μl/head of SDS sample buffer using a motor-driven pestle. After centrifugation at 16,000 g for 10 min, the supernatant was used in SDS-PAGE.

In Vitro Phosphorylation Assay

Recombinant 2x GST-dPINK1 (153–709 aa), which has an N-terminal GST-tag and a C-terminal GST/6x His tag, was produced in the *E. coli* strain pG-KJE8/BL21 (TAKARA) and purified by a sequential purification with Ni-NTA agarose and glutathione sepharose. GST-hPGAM5-S (1–255 aa) and GST-hPGAM5 (1–289 aa) were incubated with 2x GST-dPINK1 as described in Figure 2.

Whole-Mount Immunostaining and Transmission Electron Microscopic (TEM) Analysis

Counting of TH-positive neurons was performed by whole-mount immunostaining of brain samples as described previously [9]. TEM images were obtained at the Biomedical Research Core of Tohoku University Graduate School of Medicine. All histochemical analyses were performed using DeltaVision microscope system (Applied Precision) or LSM5 PASCAL laser scanning microscope system (Carl Zeiss). The images obtained by DeltaVision system were deconvolved through 10 iterations using the DeltaVision deconvolution software (Applied Precision). Area calculation of the mitochondria was performed following established criteria for classification [12] using softWoRx (Applied Precision) or Image J software from the US National Institute of Health (http//rsb.info.nih.gov/ij/).

Lifespan Assay and Quantification of Wing Phenotypes and Climbing Ability

For lifespan studies, twenty female adult flies per vial were maintained at 25°C, transferred to fresh fly food, and scored for survival every 4 or 5 days. To control for isogeny, the $PGAM5^{NP0568}$, $PINK1^{B9}$ and $PGAM5^{1}$, $PINK1^{B9}$ alleles were backcrossed to $PINK1^{B9}$ for six generations, and $parkin^{P21}$ and $PGAM5^{NP0568}$; $parkin^{P21}$ were backcrossed to w^- wild-type background for six generations, *UAS-dPGAM5* transgenic flies were generated in the w^- genetic background and thus have matched genetic backgrounds. The lifespan of $PGAM5^{1}$ was compared in the y^- genetic background. The number of flies exhibiting defective abnormal wing posture (held-up or drooped) was determined for each genotype [9]. A climbing assay was performed as described previously [42].

Statistical Analysis

One-way repeated measures ANOVA was performed to determine significant differences among multiple groups unless otherwise indicated. If a significant result was achieved ($p<0.05$), the mean of the control and the specific test groups was analyzed using the Tukey-Kramer test. For lifespan assays, the Kaplan-Meier analysis with log-rank test was performed.

Supporting Information

Figure S1 *dPGAM5* mutant alleles. (A) $PGAM5^{NP0568}$ and $PGAM5^{1}$ mutant alleles are depicted. Boxes, exons of the *dPGAM5* gene; triangles, the positions of the transposon *NP0568* and *KG09727* insertions. Coding regions and the transcript are depicted by black and yellow boxes, respectively. (B) Quantitative RT-PCR of the *dPGAM5* transcript in homozygous *dPGAM5* mutant and RNAi lines. Expression of the *dPINK1* RNAi was induced via the *Da-GAL4* driver. Primer-binding sites for PCR are shown as arrows in (A). (C) Immunoblot analysis of dPGAM5 in the homozygous *dPGAM5* mutant, RNAi and transgenic lines. LE, longer exposure. (D) Alignment of the amino acid sequences of PGAM5 orthologues. Putative transmembrane domains are underlined in green for mammalian PGAM5 and blue for *Drosophila* PGAM5. A red arrowhead indicates the point of insertion of the transposon *NP0568*. Red underlining, sequences corresponding to the reported keap1-binding motif in human PGAM5.
Found at: doi:10.1371/journal.pgen.1001229.s001 (0.69 MB TIF)

Figure S2 Quantitative RT-PCR of the *mfn* transcript in the *mfn* RNAi lines. Expression of the *mfn* RNAi was induced via the *Da-GAL4* driver, and total RNA was purified from 3rd instar larvae because *mfn* RNAi flies exhibited a pupation-defect phenotype.
Found at: doi:10.1371/journal.pgen.1001229.s002 (0.18 MB TIF)

Figure S3 Loss of *dPGAM5* improved mitochondrial degeneration of the indirect flight muscles caused by dPINK1 inactivation. To visualize the mitochondria under a fluorescence microscopy, we used the *MHC-GAL4* driver to induce expression of a mitoGFP (green) transgene in 5-day-old adult flies with the indicated genotypes. Muscle tissue was counterstained with phalloidin (red). Integrity of the mitochondria in $PINK1^{B9}$ flies was partially restored by removal of *dPGAM5* as shown by recovery of the mitoGFP signal (green) in $PINK1^{B9}PGAM5^{1}$ flies. The genotypes are as follows: *MHC-GAL4>MitoGFP* [*wild-type*], $PGAM5^{1}/Y$; *MHC-GAL4>UAS-mitoGFP* [$PGAM5^{1}$], $PINK1^{B9}/Y$; *MHC-GAL4>UAS-mitoGFP* [$PINK1^{B9}$], $PINK1^{B9}$, $PGAM5^{1}/Y$; *MHC-GAL4>UAS-mitoGFP* [$PINK1^{B9}$, $PGAM5^{1}$].
Found at: doi:10.1371/journal.pgen.1001229.s003 (1.40 MB TIF)

Acknowledgments

We are grateful to Drs. J. Chung and G. Mardon and to the Bloomington, Kyoto, and Vienna *Drosophila* Stock Centers for flies; to Drs. A. Yasui, S. Nakajima, S. Kanno, and R. Yamato for the proteomics analysis; to H. Iwasa for TEM analyses; to S. Imai for technical supports; and to Dr. Z. Huang for providing the 2x GST-dPINK1 plasmid construct.

Author Contributions

Conceived and designed the experiments: Y Imai, T Kanao. Performed the experiments: Y Imai, T Kanao, T Sawada, Y Kobayashi, Y Moriwaki. Analyzed the data: Y Imai, T Kanao, T Sawada. Contributed reagents/materials/analysis tools: Y Moriwaki, Y Ishida, K Takeda, H Ichijo, B Lu, R Takahashi. Wrote the paper: Y Imai.

References

1. Kitada T, Asakawa S, Hattori N, Matsumine H, Yamamura Y, et al. (1998) Mutations in the parkin gene cause autosomal recessive juvenile parkinsonism. Nature 392: 605–608.
2. Valente EM, Abou-Sleiman PM, Caputo V, Muqit MM, Harvey K, et al. (2004) Hereditary early-onset Parkinson's disease caused by mutations in PINK1. Science 304: 1158–1160.
3. Unoki M, Nakamura Y (2001) Growth-suppressive effects of BPOZ and EGR2, two genes involved in the PTEN signaling pathway. Oncogene 20: 4457–4465.
4. Imai Y, Soda M, Takahashi R (2000) Parkin suppresses unfolded protein stress-induced cell death through its E3 ubiquitin-protein ligase activity. J Biol Chem 275: 35661–35664.
5. Shimura H, Hattori N, Kubo S, Mizuno Y, Asakawa S, et al. (2000) Familial Parkinson disease gene product, parkin, is a ubiquitin-protein ligase. Nat Genet 25: 302–305.
6. Zhang Y, Gao J, Chung KK, Huang H, Dawson VL, et al. (2000) Parkin functions as an E2-dependent ubiquitin- protein ligase and promotes the degradation of the synaptic vesicle-associated protein, CDCrel-1. Proc Natl Acad Sci U S A 97: 13354–13359.
7. Clark IE, Dodson MW, Jiang C, Cao JH, Huh JR, et al. (2006) Drosophila pink1 is required for mitochondrial function and interacts genetically with parkin. Nature 441: 1162–1166.
8. Park J, Lee SB, Lee S, Kim Y, Song S, et al. (2006) Mitochondrial dysfunction in Drosophila PINK1 mutants is complemented by parkin. Nature 441: 1157–1161.
9. Yang Y, Gehrke S, Imai Y, Huang Z, Ouyang Y, et al. (2006) Mitochondrial pathology and muscle and dopaminergic neuron degeneration caused by inactivation of Drosophila Pink1 is rescued by Parkin. Proc Natl Acad Sci U S A 103: 10793–10798.
10. Poole AC, Thomas RE, Andrews LA, McBride HM, Whitworth AJ, et al. (2008) The PINK1/Parkin pathway regulates mitochondrial morphology. Proc Natl Acad Sci U S A 105: 1638–1643.
11. Deng H, Dodson MW, Huang H, Guo M (2008) The Parkinson's disease genes pink1 and parkin promote mitochondrial fission and/or inhibit fusion in Drosophila. Proc Natl Acad Sci U S A 105: 14503–14508.
12. Yang Y, Ouyang Y, Yang L, Beal MF, McQuibban A, et al. (2008) Pink1 regulates mitochondrial dynamics through interaction with the fission/fusion machinery. Proc Natl Acad Sci U S A 105: 7070–7075.
13. Vives-Bauza C, Zhou C, Huang Y, Cui M, de Vries RL, et al. (2010) PINK1-dependent recruitment of Parkin to mitochondria in mitophagy. Proc Natl Acad Sci U S A 107: 378–383.
14. Geisler S, Holmstrom KM, Skujat D, Fiesel FC, Rothfuss OC, et al. (2010) PINK1/Parkin-mediated mitophagy is dependent on VDAC1 and p62/SQSTM1. Nat Cell Biol 12: 119–131.
15. Narendra DP, Jin SM, Tanaka A, Suen DF, Gautier CA, et al. (2010) PINK1 is selectively stabilized on impaired mitochondria to activate Parkin. PLoS Biol 8: e1000298. doi:10.1371/journal.pbio.1000298.
16. Ziviani E, Tao RN, Whitworth AJ (2010) Drosophila Parkin requires PINK1 for mitochondrial translocation and ubiquitinates Mitofusin. Proc Natl Acad Sci U S A 107: 5018–5023.
17. Lo SC, Hannink M (2006) PGAM5, a Bcl-XL-interacting protein, is a novel substrate for the redox-regulated Keap1-dependent ubiquitin ligase complex. J Biol Chem 281: 37893–37903.
18. Takeda K, Komuro Y, Hayakawa T, Oguchi H, Ishida Y, et al. (2009) Mitochondrial phosphoglycerate mutase 5 uses alternate catalytic activity as a protein serine/threonine phosphatase to activate ASK1. Proc Natl Acad Sci U S A 106: 12301–12305.
19. Weihofen A, Ostaszewski B, Minami Y, Selkoe DJ (2008) Pink1 Parkinson mutations, the Cdc37/Hsp90 chaperones and Parkin all influence the maturation or subcellular distribution of Pink1. Hum Mol Genet 17: 602–616.
20. Moriwaki Y, Kim YJ, Ido Y, Misawa H, Kawashima K, et al. (2008) L347P PINK1 mutant that fails to bind to Hsp90/Cdc37 chaperones is rapidly degraded in a proteasome-dependent manner. Neurosci Res 61: 43–48.
21. Lin W, Kang UJ (2008) Characterization of PINK1 processing, stability, and subcellular localization. J Neurochem 106: 464–474.
22. Takatori S, Ito G, Iwatsubo T (2008) Cytoplasmic localization and proteasomal degradation of N-terminally cleaved form of PINK1. Neurosci Lett 430: 13–17.
23. Clancy DJ, Gems D, Harshman LG, Oldham S, Stocker H, et al. (2001) Extension of life-span by loss of CHICO, a Drosophila insulin receptor substrate protein. Science 292: 104–106.
24. Lo SC, Hannink M (2008) PGAM5 tethers a ternary complex containing Keap1 and Nrf2 to mitochondria. Exp Cell Res 314: 1789–1803.
25. Beilina A, Van Der Brug M, Ahmad R, Kesavapany S, Miller DW, et al. (2005) Mutations in PTEN-induced putative kinase 1 associated with recessive parkinsonism have differential effects on protein stability. Proc Natl Acad Sci U S A 102: 5703–5708.
26. Silvestri L, Caputo V, Bellacchio E, Atorino L, Dallapiccola B, et al. (2005) Mitochondrial import and enzymatic activity of PINK1 mutants associated to recessive parkinsonism. Hum Mol Genet 14: 3477–3492.
27. Okamoto K, Shaw JM (2005) Mitochondrial morphology and dynamics in yeast and multicellular eukaryotes. Annu Rev Genet 39: 503–536.
28. Chan DC (2006) Mitochondrial fusion and fission in mammals. Annu Rev Cell Dev Biol 22: 79–99.
29. Greene JC, Whitworth AJ, Kuo I, Andrews LA, Feany MB, et al. (2003) Mitochondrial pathology and apoptotic muscle degeneration in Drosophila parkin mutants. Proc Natl Acad Sci U S A 100: 4078–4083.
30. Pesah Y, Pham T, Burgess H, Middlebrooks B, Verstreken P, et al. (2004) Drosophila parkin mutants have decreased mass and cell size and increased sensitivity to oxygen radical stress. Development 131: 2183–2194.
31. Nguyen T, Nioi P, Pickett CB (2009) The Nrf2-antioxidant response element signaling pathway and its activation by oxidative stress. J Biol Chem 284: 13291–13295.
32. Sykiotis GP, Bohmann D (2008) Keap1/Nrf2 signaling regulates oxidative stress tolerance and lifespan in Drosophila. Dev Cell 14: 76–85.
33. Mai S, Klinkenberg M, Auburger G, Bereiter-Hahn J, Jendrach M (2010) Decreased expression of Drp1 and Fis1 mediates mitochondrial elongation in senescent cells and enhances resistance to oxidative stress through PINK1. J Cell Sci 123: 917–926.
34. Gandhi S, Wood-Kaczmar A, Yao Z, Plun-Favreau H, Deas E, et al. (2009) PINK1-associated Parkinson's disease is caused by neuronal vulnerability to calcium-induced cell death. Mol Cell 33: 627–638.
35. Twig G, Elorza A, Molina AJ, Mohamed H, Wikstrom JD, et al. (2008) Fission and selective fusion govern mitochondrial segregation and elimination by autophagy. EMBO J 27: 433–446.
36. Poole AC, Thomas RE, Yu S, Vincow ES, Pallanck L (2010) The mitochondrial fusion-promoting factor mitofusin is a substrate of the PINK1/parkin pathway. PLoS ONE 5: e10054. doi:10.1371/journal.pone.0010054.
37. Sandebring A, Thomas KJ, Beilina A, van der Brug M, Cleland MM, et al. (2009) Mitochondrial alterations in PINK1 deficient cells are influenced by calcineurin-dependent dephosphorylation of dynamin-related protein 1. PLoS ONE 4: e5701. doi:10.1371/journal.pone.0005701.
38. Matsuda N, Sato S, Shiba K, Okatsu K, Saisho K, et al. (2010) PINK1 stabilized by mitochondrial depolarization recruits Parkin to damaged mitochondria and activates latent Parkin for mitophagy. J Cell Biol 189: 211–221.
39. Berman SB, Chen YB, Qi B, McCaffery JM, Rucker EB 3rd, et al. (2009) Bcl-x L increases mitochondrial fission, fusion, and biomass in neurons. J Cell Biol 184: 707–719.
40. Verstreken P, Ly CV, Venken KJ, Koh TW, Zhou Y, et al. (2005) Synaptic mitochondria are critical for mobilization of reserve pool vesicles at Drosophila neuromuscular junctions. Neuron 47: 365–378.
41. Imai Y, Soda M, Inoue H, Hattori N, Mizuno Y, et al. (2001) An unfolded putative transmembrane polypeptide, which can lead to endoplasmic reticulum stress, is a substrate of Parkin. Cell 105: 891–902.
42. Imai Y, Gehrke S, Wang HQ, Takahashi R, Hasegawa K, et al. (2008) Phosphorylation of 4E-BP by LRRK2 affects the maintenance of dopaminergic neurons in Drosophila. EMBO J 27: 2432–2443.
43. Kinoshita E, Kinoshita-Kikuta E, Takiyama K, Koike T (2006) Phosphate-binding tag, a new tool to visualize phosphorylated proteins. Mol Cell Proteomics 5: 749–757.

THE JOURNAL OF BIOLOGICAL CHEMISTRY VOL. 286, NO. 9, pp. 7619–7628, March 4, 2011

N-cadherin Regulates p38 MAPK Signaling via Association with JNK-associated Leucine Zipper Protein

IMPLICATIONS FOR NEURODEGENERATION IN ALZHEIMER DISEASE[S]

Received for publication, June 26, 2010, and in revised form, December 21, 2010 Published, JBC Papers in Press, December 22, 2010, DOI 10.1074/jbc.M110.158477

Koichi Ando[‡], Kengo Uemura[§], Akira Kuzuya[‡], Masato Maesako[¶], Megumi Asada-Utsugi[¶], Masakazu Kubota[¶], Nobuhisa Aoyagi[‡], Katsuji Yoshioka[*], Katsuya Okawa[**], Haruhisa Inoue[‡‡], Jun Kawamata[‡], Shun Shimohama[§§], Tetsuaki Arai[¶¶], Ryosuke Takahashi[‡], and Ayae Kinoshita[¶1]

From the [¶]School of Human Health Sciences, Kyoto University Graduate School of Medicine, Kyoto 606-8507, Japan, the [‡]Department of Neurology, Kyoto University Graduate School of Medicine, Kyoto 606-8507, Japan, [§]Massachusetts General Hospital, Harvard Medical School, Charlestown, Massachusetts 02129, the [*]Division of Molecular Cell Signaling, Cancer Research Institute, Kanazawa University, Kanazawa 920-1192, Japan, [**]Kyowa Hakko Kirin Co., Tokyo 100-8185, Japan, the [‡‡]Center for iPS Cell Research and Application, Kyoto University, Kyoto 606-8507, Japan, the [§§]Department of Neurology, Sapporo Medical University, Sapporo 060-8556, Japan, and the [¶¶]Tokyo Institute of Psychiatry, Tokyo 156-8585, Japan

Synaptic loss, which strongly correlates with the decline of cognitive function, is one of the pathological hallmarks of Alzheimer disease. N-cadherin is a cell adhesion molecule essential for synaptic contact and is involved in the intracellular signaling pathway at the synapse. Here we report that the functional disruption of N-cadherin-mediated cell contact activated p38 MAPK in murine primary neurons, followed by neuronal death. We further observed that treatment with $A\beta_{42}$ decreased cellular N-cadherin expression through NMDA receptors accompanied by increased phosphorylation of both p38 MAPK and Tau in murine primary neurons. Moreover, expression levels of phosphorylated p38 MAPK were negatively correlated with that of N-cadherin in human brains. Proteomic analysis of human brains identified a novel interaction between N-cadherin and JNK-associated leucine zipper protein (JLP), a scaffolding protein involved in the p38 MAPK signaling pathway. We demonstrated that N-cadherin expression had an inhibitory effect on JLP-mediated p38 MAPK signal activation by decreasing the interaction between JLP and p38 MAPK in COS7 cells. Also, this study demonstrated a novel physical and functional association between N-cadherin and p38 MAPK and suggested neuroprotective roles of cadherin-based synaptic contact. The dissociation of N-cadherin-mediated synaptic contact by Aβ may underlie the pathological basis of neurodegeneration such as neuronal death, synaptic loss, and Tau phosphorylation in Alzheimer disease brain.

Alzheimer disease (AD)[2] is pathologically characterized by the presence of amyloid β-peptide (Aβ) and neurofibrillary tangles in the neocortex and hippocampus. Insoluble Aβ fibrillar aggregates found in senile plaques have long been considered to cause the neurodegeneration of AD. On the other hand, synaptic loss is another pathological hallmark of AD, which strongly correlates with the severity of cognitive impairment better than senile plaques or neurofibrillary tangles (1). Interestingly, recent studies from AD mouse models have shown that learning impairment and synaptic dysfunction become apparent before the formation of plaques, suggesting the hypothesis that soluble Aβ causes "synaptic failure" before plaques develop and neuron death occurs (2). Converging lines of evidence suggest that natural soluble Aβ oligomers trigger synaptic loss (3). Thus, in addition to the investigation of molecular mechanisms, which develop senile plaques and neurofibrillary tangles, research focusing on synaptic dysfunction is important to clarify the earliest pathology in AD.

Presenilin (PS) 1/2 is the essential catalytic component of γ-secretase proteolytic complex (4, 5), which is responsible for the final cleavage of amyloid precursor protein to generate Aβ peptides. Mutations in PS1 have been known as the most common cause of autosomal dominant familial Alzheimer disease (6–8). Interestingly, PS1 binds to N-cadherin, which is an essential molecule for synaptic contact and is abundantly localized in hippocampal synapses (9). The cytoplasmic domain of cadherin associates with the actin cytoskeleton via β-catenin and regulates synaptic contact, synaptogenesis, and dendritic spine morphology (10, 11). In addition to the structural role as an adhesive molecule, N-cadherin plays important roles in intracellular signaling pathways such as β-catenin or Wnt signaling. Also, N-cadherin-based cell-cell adhesion activates PI3K/Akt cell survival signaling by recruiting PI3K into the N-cadherin adhesion complex (12). Further, PS1 facilitates this process by promoting cadherin/PI3K association (13). As a consequence, PS1/N-cadherin interaction at the synapse seems to be neuroprotective by facilitating the PI3K/Akt survival signaling. Recently, we demonstrated that N-cadherin promotes the cell surface expression of PS1/γ-secretase, thereby activating the PI3K/Akt/GSK3β signaling pathway (14) and that N-cadherin-mediated synaptic adhesion modulates Aβ secretion as well as $A\beta_{42/40}$ ratio via PS1/

[S] The on-line version of this article (available at http://www.jbc.org) contains supplemental Figs. S1–S5.

[1] To whom correspondence should be addressed: School of Human Health Sciences, Kyoto University Graduate School of Medicine, 53, Shogoin-kawahara-cho, Sakyo-ku, Kyoto 606-8507, Japan. Tel./Fax: 81-75-751-3969; E-mail: akinoshita@hs.med.kyoto-u.ac.jp.

[2] The abbreviations used are: AD, Alzheimer disease; Aβ, amyloid β; JLP, JNK-associated leucine zipper protein; PS, presenilin; MTT, 3-(4,5-dimethylthiazol-2-yl)-2,5-diphenyltetrazolium bromide; ANOVA, analysis of variance.

N-cadherin interactions (15). Therefore, it is plausible that N-cadherin functions not only as a synaptic adhesion molecule but also as a modulator of AD pathology by affecting Aβ production and PI3K/Akt signaling.

On the other hand, increased p38 MAPK activity is associated with the neuropathology of AD (16). For example, both p38 MAPK and its upstream kinase MKK6 are activated in AD brain tissue as demonstrated by immunohistochemistry (17, 18). Activation of the p38 MAPK signaling is also reported in an AD-relevant animal model (19). Moreover, a previous report demonstrated that Aβ employs synaptic depression to drive endocytosis of synaptic AMPA receptor by activating p38 MAPK (20). Among the MAPK family members, p38 MAPK is activated by numerous unique signals such as environmental stressors and toxins, cellular injury, growth factors, and inflammatory cytokine leading to various neuronal cell fates including apoptosis, differentiation, and proliferation. However, the relationship between p38 MAPK and N-cadherin has not been elucidated in AD pathology.

Based on the above observations, we hypothesized that disruption of N-cadherin-based cell-cell contact may up-regulate the p38 MAPK signaling, leading to the neurodegeneration of AD. We demonstrated an inverse correlation between the expression levels of phosphorylated (and thus activated) p38 MAPK and those of N-cadherin in human brains. Moreover, we showed that the disruption of N-cadherin-based contact leads to an activation of p38 MAPK signaling in murine primary neurons, followed by neuronal death. Furthermore, we performed proteomic analysis using human brains and identified JNK-associated leucine zipper protein (JLP) as a novel interacting protein of N-cadherin, thus demonstrating a new signaling pathway from N-cadherin to p38 MAPK through the association with JLP, which might be compromised in AD pathogenesis.

EXPERIMENTAL PROCEDURES

Human Material and Proteomics—Human brain tissues were provided by the Tokyo Institute of Psychiatry. Brains from non-AD and AD patients were dissolved in radioimmune precipitation assay buffer (50 mM Tris, pH 8.0, 1% Triton X-100, 0.1% SDS, 150 mM NaCl, 1% Nonidet P-40, and 0.5% deoxycholate) supplemented with protease inhibitor mixture (Roche Applied Science) and phosphatase inhibitor mixture (Sigma). Each sample was then centrifuged at 14,000 × *g* for 20 min at 4 °C, and the supernatants were collected to obtain soluble proteins. Protein concentration was determined using the Bradford assay. Equal amounts of protein were subjected to SDS-PAGE followed by Western blot. For proteomic analysis, equal amounts of aliquots were treated with protein G-Sepharose (GE Healthcare) for 1 h at 4 °C. After removing protein G-Sepharose by centrifugation at 2,000 × *g* for 5 min, anti-N-cadherin antibody (BD Biosciences) was added to the supernatants. Each sample was rotated for 2 h at 4 °C and then treated with protein G-Sepharose for 1 h at 4 °C. The immunoprecipitates were washed with radioimmune precipitation assay buffer five times and resuspended in 2× sample buffer (125 mM Tris-HCl, pH 6.8, 4.3% SDS, 30% glycerol, 10% 2-mercaptoethanol, and 0.01% bromphenol blue). After boiling for 4 min, the supernatants were subjected to SDS-PAGE. To visualize proteins, the gels were stained with silver nitrate using PlusOne silver staining kit protein (GE Healthcare). The protein bands were excised and subjected to in gel trypsinization, and molecular mass analysis of the tryptic peptides was performed by MALDI-TOF/MS with an Ultraflex MALDI-TOF/TOF system (Bruker Daltonics, Billerica, MA).

Cells, Plasmids, and Transfection—HEK293 and COS7 cells were maintained in DMEM (Sigma) containing 10% FBS (Invitrogen) and 1% penicillin/streptomycin at 37 °C in a 5% CO_2 incubator. SH-SY5Y cells, which are derived from human neuroblastoma cell lines, were maintained in Opti-MEM® (Invitrogen) containing 10% FBS. Primary neurons were obtained from the cerebral cortices of fetal mice (14–16 days of gestation) and cultured in neurobasal medium supplemented with B-27 (Invitrogen). Expression plasmids encoding S-tagged JLP and its mutant derivatives were kind gifts from Dr. Reddy (Temple University) (21). FLAG-tagged p38 MAPK and FLAG-tagged MKK4 (SEK1) were described previously (22). HA-tagged MEKK3 (Addgene plasmid 12186) was provided by Dr. Johnson (National Jewish Center for Immunology and Respiratory Medicine) (23). HA-tagged N-cadherin was described elsewhere (14). Transfection of either HEK293 or COS7 cells was carried out using Transfectin reagent (Bio-Rad) according to the manufacturer's protocol.

Antibodies and Reagents—The following antibodies were used in the study: mouse monoclonal antibody to N-cadherin (BD Biosciences), rabbit polyclonal antibody to JLP (Abcam), rabbit polyclonal antibody to p38 and phospho-p38 (Cell Signaling Technology), rabbit polyclonal antibody to S-probe (Santa Cruz Biotechnology), monoclonal and rabbit polyclonal anti-HA antibodies, mouse monoclonal anti-N-cadherin N terminus antibody (N-cadherin neutralizing antibody, GC-4), anti-β-actin antibody, anti-FLAG-M2 antibody, control normal mouse IgG (Sigma), mouse monoclonal antibody to PHF-Tau (AT8) (Pierce), and Alexa Fluor 546 goat anti-rabbit IgG conjugate and Alexa Fluor 488 goat anti-mouse IgG conjugate (Molecular Probe). ADH-1 was a kind gift from Dr. Gupta (Adherex Technologies Inc.). Synthetic $A\beta_{42}$ peptides were obtained from Peptide Institute Inc. SB203580 was purchased from Calbiochem. S-protein-agarose beads were from Novagen.

Western Blot, Immunoprecipitation, Pulldown Assay, MTT Assay, and Cell Treatment by Reagents—Preparation of protein samples, Western blot, and immunoprecipitation were carried out as described elsewhere (14). Pull-down assay using S-protein-agarose beads (Novagen) was carried out as described elsewhere (21). MTT assay was performed using the MTT cell proliferation assay kit (Cayman) according to the manufacturer's instructions. For inhibition of N-cadherin-mediated cell-cell contact, the cells were treated either with ADH-1 as indicated or with N-cadherin-neutralizing antibody (GC-4) as described elsewhere (15).

Immunostaining—The samples for immunostaining were prepared as described elsewhere (15). After fixation, the samples were examined using a laser scanning confocal microscope, LSM 510 META (Zeiss).

TABLE 1
Characteristics of human cases
Clinical and histopathological information on brain samples used for analysis in Fig. 1A. We analyzed five AD patient brains confirmed by neuropathology and five control subjects without neurological complications. There is no statistical difference in age between AD and control cases. NA, not available. NFT, neurofibrillary tangle.

Case	Age	Sex	Post-mortem interval	Clinical diagnosis	Pathological findings
	years		*h*		
Non-AD					
Case 1	60	Male	NA	Alcoholism	Plaque(−), NFT stage I
Case 2	80	Female	NA	Abdominal aortic aneurysm rupture	Plaque(−), NFT stage II
Case 3	77	Male	7.5	Liver cirrhosis	Plaque(−), NFT stage II
Case 4	66	Male	11	Rectal cancer	Plaque(−), NFT stage I
Case 5	48	Male	10	Familial idiopathic basal ganglia calcification	Plaque(−), tangle(−)
AD					
Case 1	75	Male	12	Alzheimer disease	Braak stage C, VI
Case 2	68	Female	9	Alzheimer disease	Braak stage C, VI
Case 3	75	Male	17.5	Alzheimer disease	Braak stage C, VI
Case 4	81	Female	61	Dementia with Levy bodies	Alzheimer disease Braak stage C, VI
Case 5	56	Male	18	Alzheimer disease	Braak stage C, VI

Statistical Analysis—Signals on films were quantified with National Institutes of Health Image software (National Institutes of Health). Comparisons were performed using a Mann-Whitney *U* test or a Student's *t* test. For comparison of multiparametric analysis, one-way ANOVA, followed by the post hoc analysis by Fisher's protected least significant difference (PLSD) was used. Pearson's correlation co-efficients and significance were defined by STATVIEW software. The data are expressed as the means ± S.E., and statistical significance was assessed at $p < 0.05$.

RESULTS

The Expression Levels of Phosphorylated p38 MAPK Were Negatively Correlated with N-cadherin Expression Levels in Human Brains—N-cadherin is an essential adhesion molecule for forming synapses, and synaptic loss is one of pathological hallmarks of AD. Because previous reports showed that synaptic proteins such as synaptophysin or PSD-95 were reduced in AD (24, 25), we hypothesized that N-cadherin expression is also decreased in the brains of AD patients. First, the expression levels of N-cadherin were analyzed in human brain tissues from temporal cortices of AD patients and age-matched non-AD controls (Table 1). As expected, Western blot analysis using anti-N-cadherin antibody showed that expression levels of N-cadherin were decreased in AD brains compared with non-AD controls (Fig. 1*A*). Quantitative analysis showed that the ratio of N-cadherin/β-actin was significantly decreased in AD brains compared with that in non-AD controls (Fig. 1*B*, $p < 0.05$). To investigate whether the phosphorylation of p38 MAPK was enhanced in AD brains, we subsequently examined the expression levels of both phosphorylated and total p38 MAPK in the same tissues of human brains by Western blot (Fig. 1*A*). Consistent with previous reports (18–20), quantitative analysis showed a significant increase in the ratio of phospho/total p38 MAPK in AD brains, compared with that in non-AD controls (Fig. 1*C*, $p < 0.01$). Moreover, when we plotted the ratio of phospho/total p38 MAPK against that of N-cadherin/β-actin, we found that the phospho/total p38 MAPK ratio negatively correlated with N-cadherin/β-actin ratio (Fig. 1*D*, $r = -0.774$, $p < 0.01$). These results suggested a negative correlation between phosphorylated p38 MAPK and N-cadherin expressions in human brain.

ADH-1 (N-cadherin Antagonist) Induced Neuronal Cell Death by Activating p38 MAPK in Murine Primary Neurons—To elucidate the link between the reduced level of N-cadherin and p38 MAPK activation in AD brains, we analyzed whether the inhibition of N-cadherin-based synaptic contact could lead to p38 MAPK activation in neuronal cells. The N-terminal extracellular domain of N-cadherin harbors the homophilic cell adhesion recognition sequence, His-Ala-Val (HAV). It has been established that ADH-1, which mimics the natural HAV sequence of N-cadherin, can specifically disrupt N-cadherin-mediated cell adhesion (26). Therefore, we used it as a specific N-cadherin antagonist in the present experiment. First, murine primary neurons were treated with different concentrations of ADH-1 to disrupt the N-cadherin-based synaptic contact, followed by analysis of p38 MAPK activation by Western blot. Interestingly, exposure of murine primary neurons to ADH-1 for 24 h enhanced the phosphorylation of p38 MAPK and Tau in a concentration-dependent manner (Fig. 2*A* and supplemental Fig. S1). To confirm the effect of N-cadherin inhibition on p38 MAPK signaling and Tau phosphorylation in an alternative way, we applied N-cadherin-neutralizing antibody to murine primary neurons for 6 h followed by Western blot, and the same result was obtained as ADH-1 (supplemental Fig. S2). Next, we asked whether activation of p38 MAPK after inhibition of N-cadherin-based synaptic contact could lead to neuronal death. To answer this question, we examined neuronal cell viability after ADH-1 treatment using MTT assay. We observed significant decreases in neuronal cell viability after treatment with ADH-1 ($n = 4$, $p < 0.001$) (Fig. 2*B*). To evaluate whether p38 MAPK plays an important role in ADH-1-induced neuronal death, we used SB203580, a well characterized p38 MAPK-specific inhibitor. ADH-1 application with or without SB203580 revealed that neuronal death induced by ADH-1 was significantly attenuated by co-treatment with SB203580 ($n = 4$, $p < 0.001$) (Fig. 2*C*). Thus, the increased level of p38 MAPK activation is responsible for the ADH-1-induced neuronal death. To prove the effect of ADH-1 on the structural integrity of N-cadherin-mediated cell contact and p38 MAPK activation, ADH-1 (0.5 mg/ml) was added to confluent SH-SY5Y cells for 24 h. As expected, confocal microscopic analysis showed that

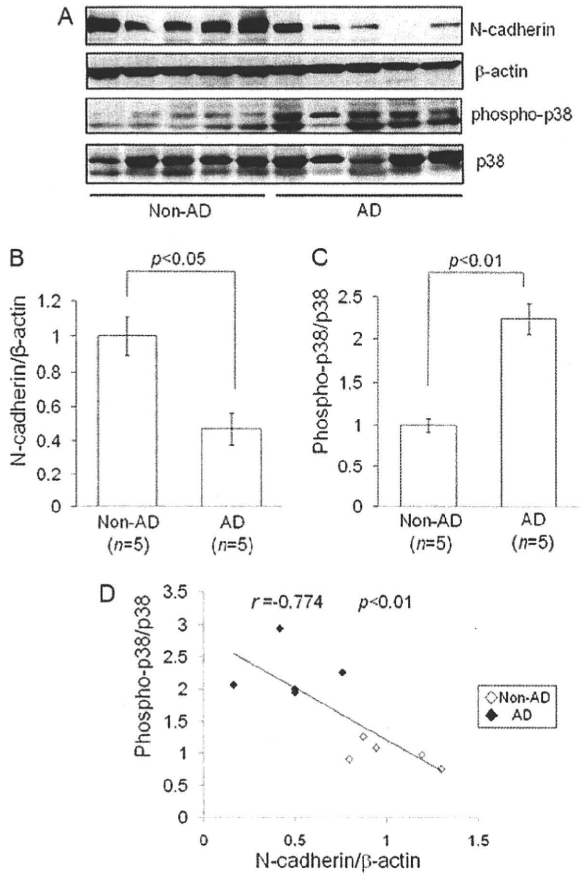

FIGURE 1. **Increased phospho-p38 MAPK expressions were negatively correlated with decreased N-cadherin expressions in human brains.** *A*, brain homogenates of temporal cortex from AD patients (*AD*, $n = 5$) and age-matched non-AD controls (*Non-AD*, $n = 5$) were analyzed by Western blot using anti-N-cadherin, β-actin, phospho-p38, and p38 MAPK antibodies. *B*, the band densities of N-cadherin and control β-actin were quantified by National Institutes of Health Image. The ratio of N-cadherin to β-actin (*N-cadherin/β-actin*) was calculated and analyzed by Mann-Whitney's *U* test. The N-cadherin/β-actin ratio was significantly decreased in the brains of AD patients compared with that of non-AD controls ($p < 0.05$). *C*, the band densities of phospho-p38 and p38 MAPK were quantified by National Institutes of Health Image. The phospho/total p38 MAPK ratio was calculated and analyzed by Mann-Whitney's *U* test. The phospho/total p38 MAPK ratio was significantly increased in the brains of AD patients compared with that of non-AD controls ($p < 0.01$). *D*, significant correlation was established in comparison between the phospho/total p38 MAPK ratio and the N-cadherin/β-actin ratio by Pearson's correlation co-efficients. The phospho/total p38 MAPK ratio was negatively correlated with the N-cadherin/β-actin ratio in human brain samples. ($r = -0.774$, $p < 0.01$).

the treatment with ADH-1 resulted in the significant decrease of N-cadherin immunoreactivity at the sites of cell-cell contact (Fig. 2*D*, *left panels*), indicating the disruption of N-cadherin-mediated cell contact. Consistent with the above result, enhanced immunoreactivity of phospho-p38 MAPK was observed in cells treated with ADH-1, compared with non-treated cells (Fig. 2*D*, *middle panels*). No immunoreactivities of both N-cadherin and phospho-p38 MAPK were observed in the absence of primary antibodies (supplemental Fig. S3).

$A\beta_{42}$ Decreased N-cadherin Expression through NMDA Receptors in Murine Primary Neurons—A number of recent studies have found that Aβ is synaptotoxic (20, 27). Therefore, we next examined whether Aβ could down-regulate N-cadherin expression in neurons. To assess the effect of Aβ on N-cadherin expressions, murine primary neurons were treated with synthetic $A\beta_{42}$ peptides (100 nM) for 48 h and subjected to Western blot. As shown in Fig. 3*A*, $A\beta_{42}$ treatment decreased N-cadherin expression in neurons. Previous reports have demonstrated that p38 MAPK is activated by the fibrillar Aβ (28) and that p38 MAPK can phosphorylate Tau at Ser-202/Thr-205 (29). Thus, we examined whether synthetic $A\beta_{42}$ peptides could trigger p38 MAPK activation and Tau phosphorylation at Ser-202/Thr-205 in our system. Consistent with the previous reports, we observed increased levels of phosphorylated p38 MAPK and phosphorylated Tau in the $A\beta_{42}$-treated cell preparations as compared with nontreated ones by Western blot ($n = 3$, $p < 0.01$) (Fig. 3, *A* and *B*). Together, this experiment indicated that $A\beta_{42}$ treatment decreases the levels of N-cadherin, activates p38 MAPK, and phosphorylates Tau in neuronal cells. Previous reports demonstrated that Aβ treatment induces excessive excitation of glutamate receptors to cause excitotoxicity (30, 31). Thus, we hypothesized that the decreased level of N-cadherin was induced by the Aβ-mediated excitotoxicity. To test this, murine primary neurons were pretreated (30 min) with the NMDA receptor antagonist MK-801 (10 μM) before being exposed to $A\beta_{42}$. Subsequent Western blot analysis of cell lysates revealed that MK-801 inhibited $A\beta_{42}$-induced reduction of N-cadherin levels ($n = 3$, $p < 0.05$) (Fig. 3*C*).

N-cadherin Associates with JLP Both in Human Brains and in Murine Primary Neurons—To clarify the mechanistic link between the disruption of N-cadherin-based contact and p38 MAPK activation, we set out to identify the proteins that associate with N-cadherin in human brain samples. For this, lysates of temporal cortices from brains of AD and non-AD patients were immunoprecipitated with anti-N-cadherin antibody, and the immunoprecipitates were subsequently subjected to SDS-PAGE. The separated proteins were visualized by silver staining, demonstrating a protein band of ~180 kDa in the lysates of brains of both AD patients and non-AD controls (supplemental Fig. S4). The protein band was identified by mass spectrometry as JLP, a scaffold protein that has been known to mediate the interaction between p38 MAPK and its upstream kinases (21). To confirm the association between N-cadherin and JLP, we transiently transfected HA-tagged N-cadherin and/or FLAG-tagged JLP expression constructs into HEK293 cells. Equal amounts of cell lysates obtained from each transfected cell were immunoprecipitated with anti-HA antibody and then immunoblotted with anti-FLAG antibody (Fig. 4*A*). A protein band of ~180 kDa was visualized with anti-FLAG antibody in the immunoprecipitate using anti-HA antibody obtained from the double-transfected cells (Fig. 4*A*, *third lane*), clearly indicating that N-cadherin associates with JLP. To further verify this association, the lysates derived from HEK293 cells transiently transfected with HA-tagged N-cadherin and/or FLAG-tagged JLP plasmids were immunoprecipitated with anti-FLAG antibody. As shown in Fig. 4*B*, HA-tagged immunoreactivity was observed in the immunoprecipitate with anti-FLAG antibody, confirming the association of N-cadherin with JLP. Finally, to demonstrate the endogenous association between N-cadherin and JLP in

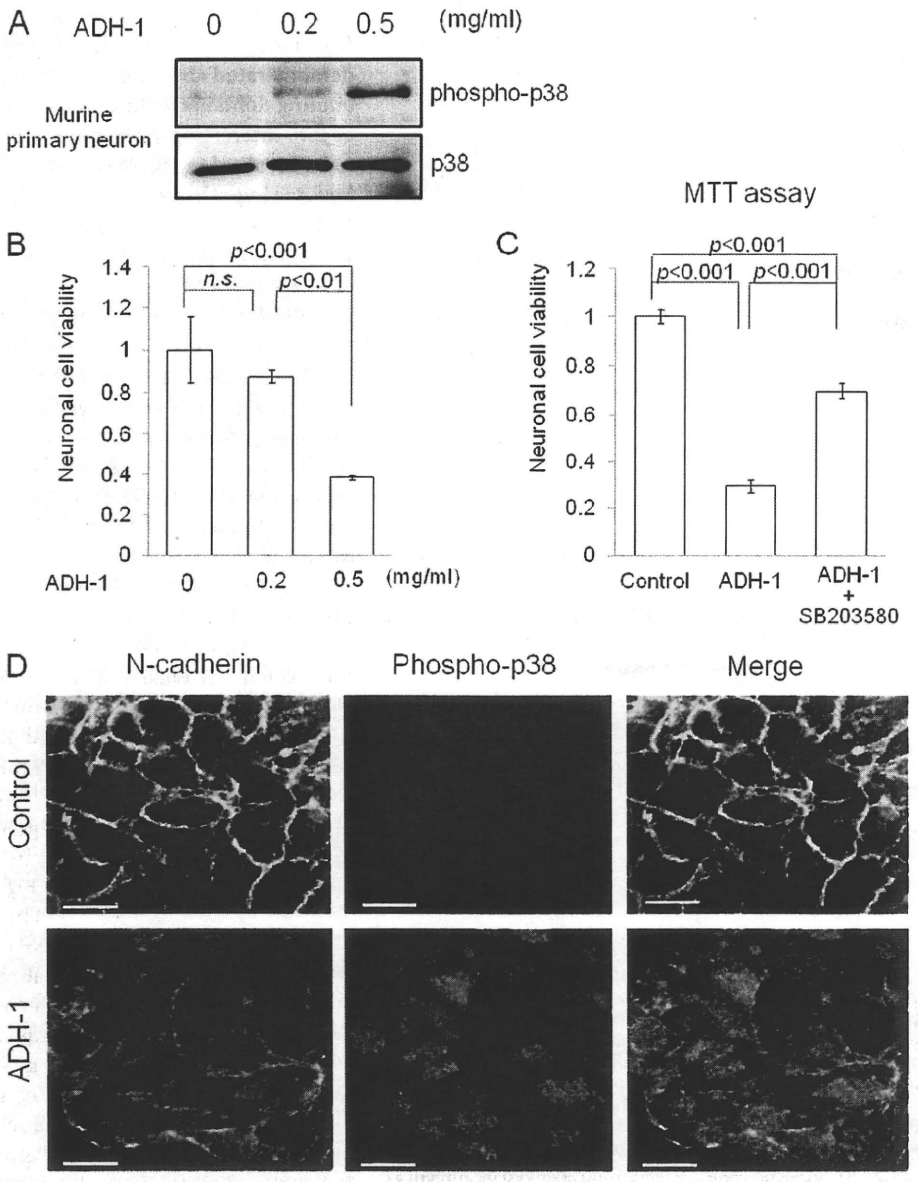

FIGURE 2. **ADH-1 induced neuronal cell death by activating p38 MAPK in murine primary neurons.** *A*, ADH-1, N-cadherin antagonist, was applied to murine primary neurons at different concentrations as shown. 24 h after treatment, the lysates were immunoblotted with anti-phospho-p38 and p38 MAPK antibodies. ADH-1 increased phosphorylation of p38 MAPK. *B*, neuronal cell death induced by ADH-1 was evaluated by MTT assay ($n = 5, p < 0.001$). *C*, murine primary neurons were treated with ADH-1 (0.5 mg/ml) for 24 h with or without 30 min of pretreatment with 10 μM SB203580, a specific p38 MAPK inhibitor, and the cell death was examined by MTT assay ($n = 4, p < 0.001$). SB203580 attenuated neuronal cell death induced by ADH-1 ($n = 4, p < 0.001$). *D*, ADH-1 (0.5 mg/ml) was added to confluent SH-SY5Y cells for 24 h followed by the immunostaining, using anti-N-cadherin and anti-phospho-p38 antibodies. Treatment with ADH-1 perturbed N-cadherin immunoreactivity, indicating a partial loss of N-cadherin from cell-cell junctions. *Scale bar*, 10 μm.

neurons, murine primary neurons were lysed, immunoprecipitated with anti-N-cadherin antibody, and then subjected to Western blot with anti-JLP antibody (Fig. 4*C*). The result showed endogenous association between N-cadherin and JLP in murine primary neurons, as well as in human brains.

N-cadherin/JLP Association Is Mediated by the Region Spanning Amino Acids 160–209 and Leucine Zipper II Domain of JLP—To determine the N-cadherin-binding domains of JLP, a series of S-tagged JLP mutants truncated at the C terminus was transfected into COS7 cells (Fig. 5*A*). Immunoprecipitation with anti-N-cadherin antibody showed that all of the S-tagged C-terminal deletion mutants of JLP were associated with N-cadherin (Fig. 5*B*), indicating that the JLP N terminus plays an important role in the association with N-cadherin. To further characterize the sequences of JLP involved in this association, various N-terminally truncated JLP mutants tagged with the S-sequence were prepared as indicated (Fig. 5*C*). COS7 cells were transiently transfected with these deletion mutants, and the lysate derived from each transfected cell was subjected to immunoprecipitation assay with anti-N-cadherin antibody. We observed that the JLP fragment corresponding to the region of amino acids 160-463 was strongly associated with N-cadherin, whereas that corresponding to the region of amino acids 160–398 showed a weaker association with N-cadherin (Fig. 5*D*). In contrast, a shorter fragment corresponding to the region of amino

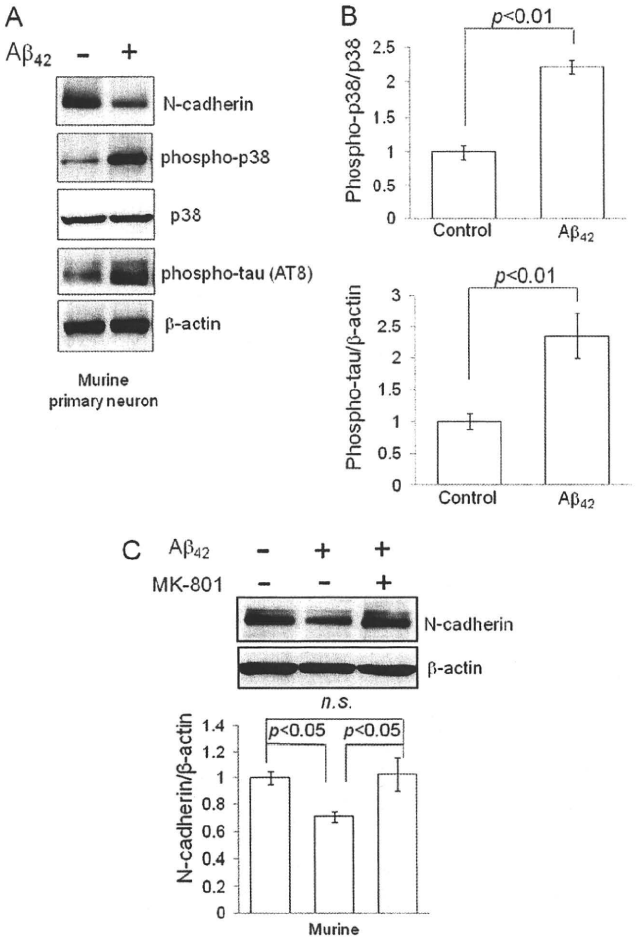

FIGURE 3. **$A\beta_{42}$ decreased N-cadherin expressions through NMDA receptors in murine primary neurons.** *A*, murine primary neurons were treated with or without 100 nM synthetic $A\beta_{42}$ peptides for 48 h, and the lysates were immunoblotted with anti-N-cadherin, phospho-p38, p38 MAPK, phospho-Tau (AT8), and β-actin antibodies, successively. $A\beta_{42}$ treatment reduced N-cadherin expressions and induced phosphorylation of p38 MAPK and Tau in murine primary neurons. *B*, the band densities of phospho-p38, p38 MAPK, phospho-Tau (AT8), and β-actin were quantified by National Institutes of Health Image. The ratios of phospho/total p38 MAPK and phospho-Tau (AT8)/β-actin were calculated and analyzed by Student's *t* test ($n = 3$, $p < 0.01$). *C*, murine primary neurons were pretreated with 10 μM MK-801, NMDA receptor antagonist for 30 min followed by 100 nM synthetic $A\beta_{42}$ peptides for 48 h. The lysates were evaluated by Western blot using anti-N-cadherin and β-actin antibodies. The band densities of N-cadherin and β-actin were quantified by National Institutes of Health Image. The N-cadherin/β-actin ratio was calculated and analyzed by one-way ANOVA. NMDA receptor antagonist MK-801 prevented the $A\beta_{42}$-induced decrease in N-cadherin levels ($n = 3$, $p < 0.05$).

acids 210–398, lacking amino acids 160–209 and leucine zipper II domain of amino acids 398–463, failed to co-immunoprecipitate with N-cadherin. These results implicated that both the region containing amino acids 160–209 and leucine zipper II domain in JLP are essential for its association with N-cadherin.

N-cadherin Expression Had a Negative Effect on p38 MAPK Activation by Inhibiting JLP/p38 MAPK Association—We next focused on investigating the functional role of the molecular association between N-cadherin and JLP. Previously, JLP has been reported to act as a scaffolding protein to bring p38 MAPK together with their upstream kinases MKK4 and MEKK3 (21), thereby activating the p38 MAPK pathway. As demonstrated above, we found that one of the N-cadherin-binding domains is the region spanning amino acids 160–209 of JLP. Interestingly, the same JLP domain has been identified to be involved in the association with p38 MAPK (21). Therefore, we hypothesized that N-cadherin could regulate the p38 MAPK signaling pathway via modulating JLP-p38 MAPK association. To prove this hypothesis, we investigated the effect of N-cadherin expression on the p38 MAPK signaling pathway in COS7 cells. FLAG-tagged p38 MAPK was transiently co-transfected into COS7 cells together with FLAG-tagged MKK4, S-tagged JLP, and HA-tagged N-cadherin as designated in Fig. 6*A*. The cell lysates were analyzed by immunoblotting with anti-phospho-p38 MAPK or p38 MAPK antibodies, respectively (Fig. 6*A*). Consistent with the previous report, the phosphorylation of p38 MAPK was enhanced by the co-expression of JLP and MKK4, upstream kinase for p38 MAPK ($n = 3$, $p < 0.05$). Interestingly, we found that this activation of p38 MAPK induced by the co-expression of MKK4 and JLP was significantly suppressed by the co-expression of N-cadherin ($n = 3$, $p < 0.05$). Alternatively, we co-transfected HA-tagged MEKK3, another upstream kinase of p38 MAPK, into COS7 cells. Similarly, we observed that the enhancement of phosphorylated p38 MAPK under the co-expression of both MEKK3 and JLP was significantly suppressed by the co-expression of N-cadherin (Fig. 6*B*, $n = 3$, $p < 0.05$). Moreover, when we pull down JLP with S-agarose, we found a reduced interaction between JLP and p38 MAPK in the presence of N-cadherin (Fig. 6), indicating that N-cadherin competitively inhibits the binding of p38 MAPK to JLP. Indeed, co-transfection of FLAG-tagged p38 MAPK, FLAG-tagged MKK4, and JLP fragment corresponding to the region of amino acids 160–463, which could associate with N-cadherin into COS7 cells, showed the increased phosphorylation of p38 MAPK (supplemental Fig. S5). This result implies that this short fragment of JLP may compete with the endogenous JLP for the N-cadherin binding, resulting in the release of JLP from the N-cadherin and subsequent p38 MAPK activation. Taken together, these results suggested that N-cadherin expression had an inhibitory effect on the p38 MAPK signaling pathway via inhibition of JLP-p38 MAPK association.

DISCUSSION

The molecular mechanism of synaptic adhesion and cell viability pathway of p38 MAPK is not well understood yet. Our present study suggested a potentially new signaling pathway contributing to the aberrant activation of p38 MAPK in AD. We showed that ADH-1 caused a significant increase in p38 MAPK activation and Tau phosphorylation with a subsequent decrease in neuronal viability (Fig. 2, *A* and *B*, and supplemental Fig. S1). In alternative ways, application of N-cadherin-neutralizing antibody also activated p38 MAPK and increased phosphorylation of Tau in murine primary neurons (supplemental Fig. S2), suggesting that the disruption of N-cadherin-based cell adhesion could lead to p38 MAPK activation and Tau phosphorylation. Importantly, we demonstrated that the inhibition of the p38 MAPK pathway with specific

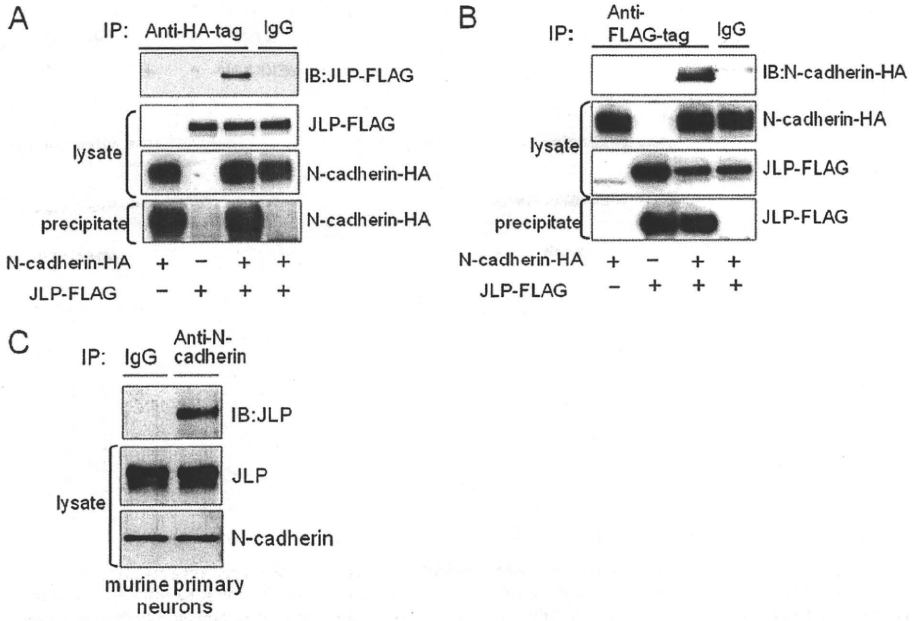

FIGURE 4. **The association of N-cadherin with JLP in HEK293 cells and neuronal cells.** *A*, lysates of HEK293 cells, transiently transfected with HA-tagged N-cadherin and/or FLAG-tagged JLP expressing vectors, were immunoprecipitated (*IP*) with anti-HA antibody (*lanes 1–3*) or normal IgG (*lane 4*). The immunoprecipitates and the lysates were analyzed by immunoblotting (*IB*) with the specific antibodies against the FLAG tag and HA tag. *B*, lysates of HEK293 cells, transiently transfected with HA-tagged N-cadherin and/or FLAG-tagged JLP expressing vectors were immunoprecipitated with anti-FLAG antibody (*lanes 1–3*) or normal IgG (*lane 4*). The immunoprecipitates and the lysates were analyzed by Western blot with the specific antibodies against the HA tag and FLAG tag. *C*, the endogenous association between N-cadherin and JLP in murine primary neurons was analyzed. The neurons were lysed and immunoprecipitated with either anti-N-cadherin antibody or normal IgG. The immunoprecipitates and the lysates were immunoblotted with the specific antibodies against JLP and N-cadherin.

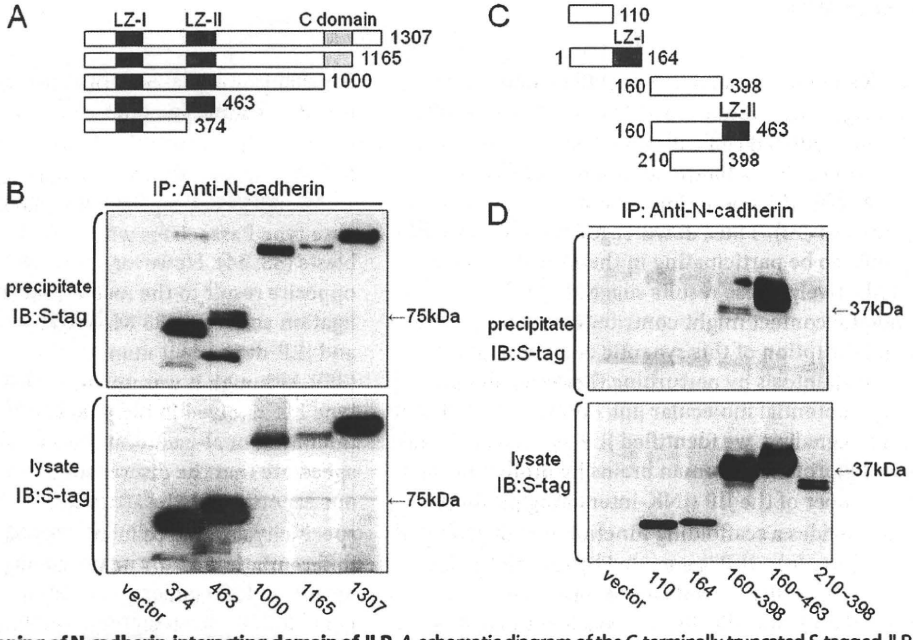

FIGURE 5. **Deletion mapping of N-cadherin-interacting domain of JLP.** *A*, schematic diagram of the C-terminally truncated S-tagged JLP constructs used for analysis of the JLP-N-cadherin interaction. The sizes of these deletion mutants were 374 (amino acids 1–374), 467 (amino acids 1–467), 1000 (amino acids 1–1000), 1165 (amino acids 1–1165), and 1307 amino acids (full length, residues 1–1307), respectively. *B*, COS7 cells were transiently transfected with the WT or C-terminally truncated mutants of S-tagged JLP. The lysates were immunoprecipitated (*IP*) with anti-N-cadherin antibody. The immunoprecipitates and the lysates were subjected to Western blot analysis with the specific antibodies against S-tag. All of these deletion mutants of JLP were co-immunoprecipitated with N-cadherin. *C*, schematic diagram representing shorter constructs of C-terminally truncated S-tagged JLP. N-terminally truncated short constructs were also prepared as shown in Fig. 5*C*. *D*, COS7 cells were transiently transfected with these different mutants of S-tagged JLP. The lysates were immunoprecipitated with anti-N-cadherin antibody, and the immunoprecipitates were immunoblotted (*IB*) with anti-S-tag antibody. The mutants consisting of amino acids 160–398 and 160–463 of JLP were co-immunoprecipitated with N-cadherin, whereas the mutant consisting of amino acids 210–398 of JLP was not co-immunoprecipitated with N-cadherin.

p38 MAPK inhibitor (SB203580) attenuated ADH-1-induced neurotoxicity (Fig. 2*C*), indicating an important role of p38 MAPK in the cell death caused by the inhibition of N-cadherin-based cell adhesion. However, because the application of SB203580 did not block ADH-1-induced cell death completely, we assume that other alterations in cellular signaling

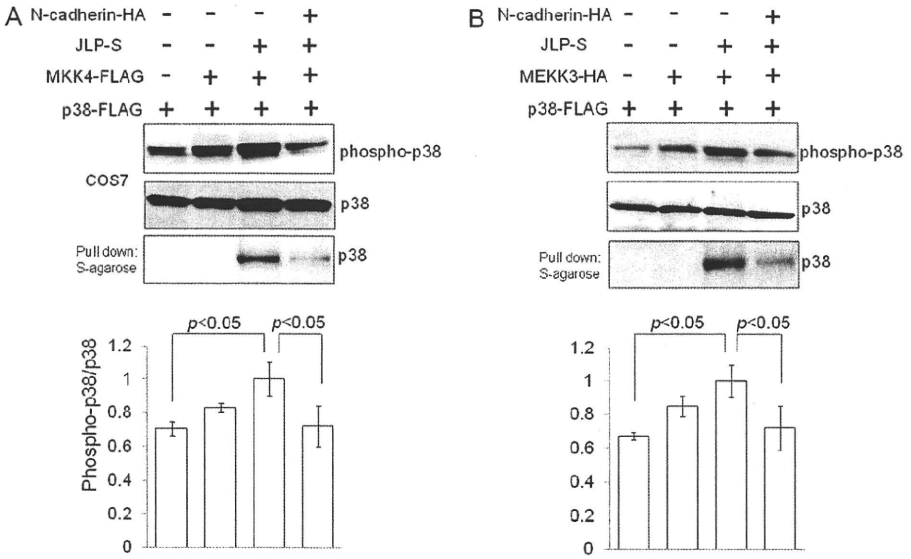

FIGURE 6. **N-cadherin expression inhibited JLP-associated p38 MAPK pathway.** *A*, COS7 cells were co-transfected with FLAG-tagged p38α, FLAG-tagged MKK4, S-tagged JLP, and HA-tagged N-cadherin. 24 h after transfection, the lysates were precipitated with S-protein-agarose. The lysates and precipitates were subjected to Western blot analysis with anti-phospho-p38 or p38 MAPK antibodies. One representative immunoblot result is shown. The band densities of phospho-p38 and p38 MAPK were quantified by National Institutes of Health Image. The phospho/total p38 MAPK ratio was calculated and analyzed by one-way ANOVA. N-cadherin expression significantly inhibited JLP/MKK4-mediated phosphorylation of p38 MAPK compared with that without expression of N-cadherin ($n = 3$, $p < 0.05$). Pull-down assay using S-protein-agarose showed that N-cadherin expression decreased the interaction between JLP and p38 MAPK. *B*, COS7 cells were co-transfected with FLAG-tagged p38α, HA-tagged MEKK3, S-tagged JLP, and HA-tagged N-cadherin. 24 h after transfection, the lysates were subjected to Western blot analysis with anti-phospho-p38 or p38 MAPK antibodies. One representative immunoblot result is shown. The band densities of phospho-p38 and p38 were quantified by National Institutes of Health Image. The ratio of phospho/total p38 MAPK was calculated and analyzed by one-way ANOVA. N-cadherin expression inhibited JLP/MEKK3-mediated phosphorylation of p38 MAPK significantly compared with that without expression of N-cadherin ($n = 3$, $p < 0.05$). Pull-down assay using S-protein-agarose showed that N-cadherin expression inhibited the interaction between JLP and p38 MAPK.

might be involved in neuronal death in addition to activation of p38 MAPK signaling. Notably, previous studies have shown that N-cadherin-mediated cell adhesion leads to the recruitment of PI3K into the N-cadherin adhesion complex followed by activation of Akt, which is an important regulator of anti-apoptotic pathways (12). Thus, down-regulation of PI3K/Akt signaling could also be participating in the ADH-1-induced cell death. Collectively, these results suggest that N-cadherin-mediated synaptic contact might contribute to neuroprotective signaling. Disruption of this synaptic contact might lead to neuronal cell apoptosis by perturbing these signalings.

Concerning a potential molecular link between N-cadherin and p38 MAPK signaling, we identified JLP as a novel N-cadherin-interacting protein in human brains by proteomic analysis. JLP is a member of the JIP (JNK-interacting protein) family, which provides a scaffolding function for the JNK/p38 MAPK signaling module. JLP is encoded by the *JIP4* gene, which generates three distinct splice variants, namely, JLP, JIP4, and SPAG9 (32). Specifically, JLP was identified as a scaffold protein involved in the p38 MAPK signaling pathway to bring p38 MAPK together with its upstream kinases (21). We also demonstrated that both the leucine zipper II domain and the region containing amino acids 160–209 of JLP were required for the association with N-cadherin, the same region for the interaction with p38 MAPK, which may explain the competitive regulation by N-cadherin. Moreover, our data showed that N-cadherin overexpression interfered with the physical interaction between JLP and p38 MAPK, thereby inhibiting the JLP-mediated activation of p38 MAPK signaling. Thus, it is plausible that perturbation of N-cadherin-based cell adhesion and/or reduced expression of N-cadherin could lead to aberrant activation of p38 MAPK via facilitating JLP-mediated p38 MAPK signaling.

Several recent reports have shown that cysteine dioxygenase type I associates with both N-cadherin and JLP in myoblasts (33, 34). However, our observation demonstrated an opposite result to the recent report showing that N-cadherin ligation activates p38 MAPK in a cysteine dioxygenase type I- and JLP-dependent manner during myoblast differentiation (35). Although it was unclear whether cysteine dioxygenase type I is involved in the p38 MAPK activation induced by the inhibition of N-cadherin-based cell adhesion in our study, we speculate that the discrepancy between our study and previous reports could be attributed to the differences in cell type specificity and the cellular context examined (*i.e.* myoblast differentiation *versus* neuronal degeneration). Variable roles of JLP and N-cadherin according to the differential cellular context have been demonstrated in previous studies. For example, JLP has been reported to negatively regulate NGF-induced neurite outgrowth via JNK inhibition during neuronal differentiation (36) as opposed to the previous report demonstrating that N-cadherin is involved in NGF-induced neurite outgrowth (37). Thus, the association between N-cadherin and JLP may be involved in differential cell fate by modulating signaling pathways including p38 MAPK and JNK according to the cellular context.

With respect to AD pathophysiology, the effect of Aβ on N-cadherin expression has been unclear. In this study, we

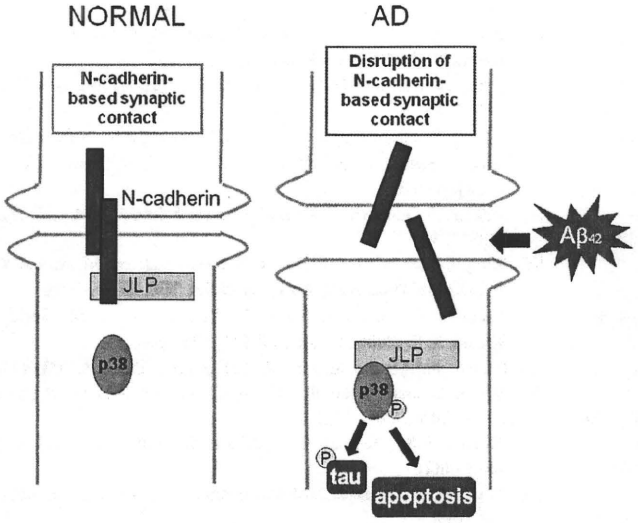

FIGURE 7. **Hypothetical model of AD pathogenesis caused by the disruption of N-cadherin-based synaptic contact.** *Left panel*, in the basal state at the synapse, N-cadherin-based synaptic adhesion stabilizes JLP, which suppresses neurotoxic p38 MAPK activation. *Right panel*, in AD, when N-cadherin-based synaptic contact is disrupted by $A\beta_{42}$, $A\beta_{42}$ could decrease N-cadherin expressions resulting in aberrant p38 MAPK activation followed by the subsequent Tau phosphorylation and neuronal death.

demonstrated that treatment with $A\beta_{42}$ decreased endogenous N-cadherin expression in murine primary neurons, whereas the aberrant phosphorylation of both p38 MAPK and p38 MAPK-sensitive Tau Ser-202/Thr-205 epitopes were simultaneously observed, as previously reported (29, 38). This result raises the possibility that $A\beta_{42}$ could interfere with N-cadherin-mediated synaptic contact, resulting in p38 MAPK activation. Recently, converging lines of evidence suggest that natural soluble $A\beta$ oligomers trigger synaptic loss (3, 20). Therefore, it is plausible that synaptic dissociation caused by $A\beta$ activates the p38 MAPK signaling pathway, leading to neuronal death as well as Tau phosphorylation. Interestingly, it has been shown that electroconvulsive and other excitatory stimuli induce arcadlin, a protocadherin, to promote activation of p38 MAPK and the endocytosis of N-cadherin at the synapse (39). Indeed, the neurodegeneration caused by $A\beta$ has long been related to the excessive activation of glutamate receptors, namely, excitotoxicity (30). Moreover, it is demonstrated that even physiological levels of $A\beta$ can enhance glutamate excitotoxicity (31). Importantly, we showed that $A\beta_{42}$-induced reduction of N-cadherin levels was NMDA receptor-dependent (Fig. 3*B*). Thus, it is possible that $A\beta$ enhances excitotoxity to promote the endocytosis of N-cadherin at the synapse, presumably followed by its degeneration by endosome/lysosome pathway. Alternatively, another group previously reported calpain-mediated degradation of N-cadherin after NMDA receptor stimulation (40). In either scenario, a decrease in N-cadherin expression could accelerate the JLP-mediated p38 MAPK activation, resulting in synaptic loss, increased phosphorylated Tau, and neuronal death in AD pathology. Overall, we suggest the possibility that JLP is a key molecule linking synaptic adhesion to p38 MAPK signaling involved in Tau phosphorylation and neuronal death associated with AD (Fig. 7).

In summary, our study suggested the physical and functional association between N-cadherin and p38 MAPK via JLP. We also demonstrated that perturbation of N-cadherin-mediated synaptic contact activated p38 MAPK pathway and increased Tau phosphorylation, leading to neuronal death. From observations obtained from the present study, we would like to extend our view of JLP function further and suggest that JLP is involved in the N-cadherin/p38 MAPK signaling pathway from synaptic adhesion to neurodegeneration. Because there were no reports focusing on the effect of $A\beta$ on synaptic adhesion, this is the first report proposing an attractive possibility that $A\beta_{42}$ may dissociate N-cadherin-mediated synaptic contact to trigger p38 MAPK activation, followed by neurodegeneration such as synaptic loss, Tau phosphorylation, and neuronal death in AD. Future study in this field could lead to a better understanding of AD pathophysiology.

Acknowledgments—We greatly thank Dr. E. P. Reddy (Temple University) for WT-JLP-S and its mutant derivatives, Dr. Johnson (National Jewish Center for Immunology and Respiratory Medicine) for MEKK3-HA, and Dr. Gupta (Adherex Technologies Inc.) for ADH-1.

REFERENCES

1. Terry, R. D., Masliah, E., Salmon, D. P., Butters, N., DeTeresa, R., Hill, R., Hansen, L. A., and Katzman, R. (1991) *Ann. Neurol.* **30,** 572–580
2. Selkoe, D. J. (2002) *Science* **298,** 789–791
3. Shankar, G. M., Bloodgood, B. L., Townsend, M., Walsh, D. M., Selkoe, D. J., and Sabatini, B. L. (2007) *J. Neurosci.* **27,** 2866–2875
4. Wolfe, M. S., De Los Angeles, J., Miller, D. D., Xia, W., and Selkoe, D. J. (1999) *Biochemistry* **38,** 11223–11230
5. Wolfe, M. S., Xia, W., Ostaszewski, B. L., Diehl, T. S., Kimberly, W. T., and Selkoe, D. J. (1999) *Nature* **398,** 513–517
6. Rogaev, E. I., Sherrington, R., Rogaeva, E. A., Levesque, G., Ikeda, M., Liang, Y., Chi, H., Lin, C., Holman, K., Tsuda, T., Mar, L., Sorbi, S., Nacmias, B., Piacentini, S., Amaducci, L., Chumakov, I., Cohen, D., Lannfelt, L., Fraser, P. E., Rommens, J. M., and St. George-Hyslop, P. H. (1995) *Nature* **376,** 775–778
7. Sherrington, R., Rogaev, E. I., Liang, Y., Rogaeva, E. A., Levesque, G., Ikeda, M., Chi, H., Lin, C., Li, G., Holman, K., Tsuda, T., Mar, L., Foncin, J. F., Bruni, A. C., Montesi, M. P., Sorbi, S., Rainero, I., Pinessi, L., Nee, L., Chumakov, I., Pollen, D., Brookes, A., Sanseau, P., Polinsky, R. J., Wasco, W., Da Silva, H. A., Haines, J. L., Perkicak-Vance, M. A., Tanzi, R. E., Roses, A. D., Fraser, P. E., Rommens, J. M., and St. George-Hyslop, P. H. (1995) *Nature* **375,** 754–760
8. Thinakaran, G. (1999) *J. Clin. Invest.* **104,** 1321–1327
9. Benson, D. L., and Tanaka, H. (1998) *J Neurosci.* **18,** 6892–6904
10. Murase, S., Mosser, E., and Schuman, E. M. (2002) *Neuron* **35,** 91–105
11. Togashi, H., Abe, K., Mizoguchi, A., Takaoka, K., Chisaka, O., and Takeichi, M. (2002) *Neuron* **35,** 77–89
12. Tran, N. L., Adams, D. G., Vaillancourt, R. R., and Heimark, R. L. (2002) *J. Biol. Chem.* **277,** 32905–32914
13. Baki, L., Shioi, J., Wen, P., Shao, Z., Schwarzman, A., Gama-Sosa, M., Neve, R., and Robakis, N. K. (2004) *EMBO J.* **23,** 2586–2596
14. Uemura, K., Kuzuya, A., Shimozono, Y., Aoyagi, N., Ando, K., Shimohama, S., and Kinoshita, A. (2007) *J. Biol. Chem.* **282,** 15823–15832
15. Uemura, K., Lill, C. M., Banks, M., Asada, M., Aoyagi, N., Ando, K., Kubota, M., Kihara, T., Nishimoto, T., Sugimoto, H., Takahashi, R., Hyman, B. T., Shimohama, S., Berezovska, O., and Kinoshita, A. (2009) *J Neurochem.* **108,** 350–360
16. Johnson, G. V., and Bailey, C. D. (2003) *Exp. Neurol.* **183,** 263–268
17. Hensley, K., Floyd, R. A., Zheng, N. Y., Nael, R., Robinson, K. A., Nguyen, X., Pye, Q. N., Stewart, C. A., Geddes, J., Markesbery, W. R.,

Patel, E., Johnson, G. V., and Bing, G. (1999) *J. Neurochem.* **72,** 2053–2058
18. Zhu, X., Rottkamp, C. A., Hartzler, A., Sun, Z., Takeda, A., Boux, H., Shimohama, S., Perry, G., and Smith, M. A. (2001) *J. Neurochem.* **79,** 311–318
19. Savage, M. J., Lin, Y. G., Ciallella, J. R., Flood, D. G., and Scott, R. W. (2002) *J. Neurosci.* **22,** 3376–3385
20. Hsieh, H., Boehm, J., Sato, C., Iwatsubo, T., Tomita, T., Sisodia, S., and Malinow, R. (2006) *Neuron* **52,** 831–843
21. Lee, C. M., Onésime, D., Reddy, C. D., Dhanasekaran, N., and Reddy, E. P. (2002) *Proc. Natl. Acad. Sci. U.S.A.* **99,** 14189–14194
22. Ito, M., Yoshioka, K., Akechi, M., Yamashita, S., Takamatsu, N., Sugiyama, K., Hibi, M., Nakabeppu, Y., Shiba, T., and Yamamoto, K. I. (1999) *Mol. Cell. Biol.* **19,** 7539–7548
23. Blank, J. L., Gerwins, P., Elliott, E. M., Sather, S., and Johnson, G. L. (1996) *J. Biol. Chem.* **271,** 5361–5368
24. Masliah, E., Terry, R. D., DeTeresa, R. M., and Hansen, L. A. (1989) *Neurosci. Lett.* **103,** 234–239
25. Gylys, K. H., Fein, J. A., Yang, F., Wiley, D. J., Miller, C. A., and Cole, G. M. (2004) *Am. J. Pathol.* **165,** 1809–1817
26. Williams, E., Williams, G., Gour, B. J., Blaschuk, O. W., and Doherty, P. (2000) *J. Biol. Chem.* **275,** 4007–4012
27. Snyder, E. M., Nong, Y., Almeida, C. G., Paul, S., Moran, T., Choi, E. Y., Nairn, A. C., Salter, M. W., Lombroso, P. J., Gouras, G. K., and Greengard, P. (2005) *Nat. Neurosci.* **8,** 1051–1058
28. Zhu, X., Mei, M., Lee, H. G., Wang, Y., Han, J., Perry, G., and Smith, M. A. (2005) *Neurochem. Res.* **30,** 791–796
29. Reynolds, C. H., Nebreda, A. R., Gibb, G. M., Utton, M. A., and Anderton, B. H. (1997) *J. Neurochem.* **69,** 191–198
30. Hynd, M. R., Scott, H. L., and Dodd, P. R. (2004) *Neurochem. Int.* **45,** 583–595
31. Kihara, T., Shimohama, S., Sawada, H., Honda, K., Nakamizo, T., Shibasaki, H., Kume, T., and Akaike, A. (2001) *J. Biol. Chem.* **276,** 13541–13546
32. Kelkar, N., Standen, C. L., and Davis, R. J. (2005) *Mol. Cell. Biol.* **25,** 2733–2743
33. Kang, J. S., Feinleib, J. L., Knox, S., Ketteringham, M. A., and Krauss, R. S. (2003) *Proc. Natl. Acad. Sci. U.S.A.* **100,** 3989–3994
34. Takaesu, G., Kang, J. S., Bae, G. U., Yi, M. J., Lee, C. M., Reddy, E. P., and Krauss, R. S. (2006) *J. Cell Biol.* **175,** 383–388
35. Lu, M., and Krauss, R. S. *Proc. Natl. Acad. Sci. U.S.A.* **107,** 4212–4217
36. Xu, H., Dhanasekaran, D. N., Lee, C. M., and Reddy, E. P. (2010) *J. Biol. Chem.* **285,** 3548–3553
37. Hansen, S. M., Berezin, V., and Bock, E. (2008) *Cell Mol. Life. Sci.* **65,** 3809–3821
38. Goedert, M., Jakes, R., and Vanmechelen, E. (1995) *Neurosci. Lett.* **189,** 167–169
39. Yasuda, S., Tanaka, H., Sugiura, H., Okamura, K., Sakaguchi, T., Tran, U., Takemiya, T., Mizoguchi, A., Yagita, Y., Sakurai, T., De Robertis, E. M., and Yamagata, K. (2007) *Neuron* **56,** 456–471
40. Jang, Y. N., Jung, Y. S., Lee, S. H., Moon, C. H., Kim, C. H., and Baik, E. J. (2009) *J Neurosci* **29,** 5974–5984

THE JOURNAL OF BIOLOGICAL CHEMISTRY VOL. 286, NO. 10, pp. 7947–7957, March 11, 2011

The Endoplasmic Reticulum Stress Sensor, ATF6α, Protects against Neurotoxin-induced Dopaminergic Neuronal Death*[S]

Received for publication, June 22, 2010, and in revised form, October 17, 2010 Published, JBC Papers in Press, December 3, 2010, DOI 10.1074/jbc.M110.156430

Naohiro Egawa[‡§], Keisuke Yamamoto[¶‖], Haruhisa Inoue[**], Rie Hikawa[‡§], Katsunori Nishi[‡‡], Kazutoshi Mori[§¶], and Ryosuke Takahashi[‡§1]

From the [‡]Department of Neurology, Graduate School of Medicine, Kyoto University, Kyoto 606-8507, Japan, [§]Core Research for Evolutional Science and Technology (CREST), Japan Science and Technology Corporation, Japan, the [¶]Department of Biophysics, Graduate School of Science, Kyoto University, Kyoto 606-8502, Japan, the [‖]Institute of Genome Research, Tokushima University, Tokushima 770-8503, Japan, the [**]Center for iPS Cell Research and Application (CiRA), Kyoto University, Kyoto 606-8507, Japan, and the [‡‡]Tokyo Metropolitan Institute for Neuroscience, Tokyo 183-8526, Japan

Oxidative stress and endoplasmic reticulum (ER) stress are thought to contribute to the pathogenesis of various neurodegenerative diseases including Parkinson disease (PD), however, the relationship between these stresses remains unclear. ATF6α is an ER-membrane-bound transcription factor that is activated by protein misfolding in the ER and functions as a critical regulator of ER quality control proteins in mammalian cells. The goal of this study was to explore the cause-effect relationship between oxidative stress and ER stress in the pathogenesis of neurotoxin-induced model of PD. 1-Methyl-4-phenyl-1,2,3,6-tetrahydropyridine (MPTP), a dopaminergic neurotoxin known to produce oxidative stress, activated ATF6α and increased ER chaperones and ER-associated degradation (ERAD) component in dopaminergic neurons. Importantly, MPTP induced formation of ubiquitin- immunopositive inclusions and loss of dopaminergic neurons more prominently in mice deficient in ATF6α than in wild-type mice. Cultured cell experiments revealed that 1-methyl-4-phenylpyridinium (MPP^+)-induced oxidative stress not only promoted phosphorylation of p38 mitogen-activated protein kinase (p38MAPK) but also enhanced interaction between phosphorylated p38MAPK and ATF6α, leading to increment in transcriptional activator activity of ATF6α. Thus, our results revealed a link between oxidative stress and ER stress by showing the importance of ATF6α in the protection of the dopaminergic neurons from MPTP that occurs through oxidative stress-induced activation of ATF6α and p38MAPK-mediated enhancement of ATF6α transcriptional activity.

Parkinson disease (PD)[2] is characterized pathologically by progressive and selective loss of dopaminergic neurons in the substantia nigra pars compacta (SNc). Recent studies have suggested some pathogenetic mechanisms of PD, including mitochondrial dysfunction (1), oxidative stress induced by dopamine metabolites, and endoplasmic reticulum (ER) stress induced by the accumulation of unfolded proteins (2–4). Dopaminergic neuron loss is often accompanied by formation of intraneuronal inclusion bodies termed Lewy bodies whose major constituent is α-synuclein (5), suggesting the pathogenetic role of unfolded protein accumulation and aggregation.

The unfolded protein response (UPR) is a homeostatic signaling pathway designed to cope with the accumulation of unfolded proteins in the ER lumen. In mammals, the UPR utilize three types of sensor proteins, PERK, IRE1α, and ATF6α, which detect protein-misfolding stress in the ER and initiate ER-to-nucleus signaling cascades to maintain the homeostasis of protein quality control system (6). ATF6 is a type 2 transmembrane protein; the C-terminal region is located in the ER, whereas the N-terminal region is located in the cytosolic side. ATF6 consists of two subtypes, ATF6α and ATF6β. ATF6α or ATF6β single knock-out mice normally develops but mice deficient in both subtypes of ATF6 genes showed embryonic lethal (7, 8). Upon ER stress the N-terminal fragment of ATF6α designated pATF6α(N) is cleaved from the parent protein designated pATF6α(P) and transported into the nucleus, where it binds to cis-acting ER stress response element (ERSE) and UPR element (UPRE), and up-regulates major ER chaperones and ER-associated degradation (ERAD) components (9–14).

1-Methyl-4-phenyl-1,2,3,6-tetrahydropyridine (MPTP) is converted into 1-methyl-4- phenylpyridinium (MPP^+) in astrocytes and taken up by dopaminergic neurons through the dopamine transporter (DAT). MPP^+ interferes with the mitochondrial complex-1, generates reactive oxygen species (ROS) and selectively damages dopaminergic neurons (15). Dopamine itself is also a highly-reactive molecule and naturally metabolized to produce ROS including hydrogen peroxide (H_2O_2) via the monoamine oxidase pathway (16). Dopamine-induced ROS promotes phosphorylation of p38 mitogen-activated protein kinase (p38MAPK) (17). MPTP activates p38MAPK pathway in the dopaminergic neuron (18). Other

* This study was supported in part by a grant-in-aid for scientific research on Priority Areas-Research on Pathomechanisms of Brain Disorders from the Ministry of Education, Culture, Sports, Science and Technology of Japan and a Grant-in-aid from the Ministry of Health, Labor, and Welfare of Japan.

[S] The on-line version of this article (available at http://www.jbc.org) contains supplemental Table S1 and Figs. S1–S3.

[1] To whom correspondence should be addressed: Dept. of Neurology, Kyoto University Graduate School of Medicine, 54 Shogoin-Kawahara-cho, Sakyo-ku, Kyoto 606-8507, Japan. Tel.: 81-75-751-3770; Fax: 81-75-761-9780; E-mail: ryosuket@kuhp.kyoto-u.ac.jp.

[2] The abbreviations used are: PD, Parkinson disease; ER, endoplasmic reticulum; MPTP, 1-methyl-4-phenyl-1,2,3,6-tetrahydropyridine; ERAD, ER-associated degradation; UPR, unfolded protein response; MPP^+, 1-methyl-4-phenylpyridinium.

oxidative neurotoxins such as rotenone and 6-hydroxydopamine (6-OHDA) also enhance the phosphorylation of p38MAPK (19, 20). Interestingly, it was previously reported that phosphorylated p38MAPK can regulate ATF6α function via phosphorylation (21), suggesting the possibility that oxidative stress and ER stress intersect at the level of p38MAPK and ATF6α.

Based on these data, the goal of the present study was to explore the cause-effect relationship between oxidative stress and ER stress in the pathogenesis of PD using ATF6α wild-type (WT) and knock-out (KO) mice treated with MPTP that causes oxidative stress and damages dopaminergic neurons.

EXPERIMENTAL PROCEDURES

Animal and MPTP Treatment—ATF6α knock-out (KO) mice were generated by gene targeting techniques as previously described (7). Groups of male ATF6α KO mice and wild-type (WT) littermate controls were injected intraperitoneal with 20 mg/kg of MPTP hydrochloride (Sigma-Aldrich) four times at 2 h intervals on the same day ($n = 10$ for each group). The mice were decapitated 5 days after injection for the subsequent analysis. All surgical procedures were performed according to the rules set forth by the Ethics Committee of Kyoto University.

Quantitative Real-time PCR—The mouse central nervous system (CNS) was dissected into the cerebral cortex, the brainstem, the hippocampus, the striatum, the midbrain, the cerebellum, the olfactory bulb, and the thalamus. Total RNA was isolated from the various parts of the CNS using the RNeasy Kit (Qiagen, Valencia CA) after homogenization (POLYTRON PT10–35). The first strand of cDNA was synthesized from 1 μg of total RNA using the PrimeScript RT Reagent Kit (Takara Bio, Shiga). Real-time PCR was performed using the LightCycler SYBR Green Master Kit and LightCycler 480 program (Roche) according to the manufacturer's protocol. The sequences of the primers used were listed in the supplemental Table S1. Values were normalized and expressed relative to GAPDH values.

Immunoblotting—Each part of the dissected CNS tissue was weighed and homogenized (POLYTRON PT10–35) in 1 ml/g of ice-cold buffer (50 mM Tris(pH7.5), 5 mM EDTA and 120 mM NaCl, 1% Triton X-100) containing protease inhibitor and phosphatase inhibitor mixture. Samples were centrifuged at 1,000 × *g* for 5 min, where the supernatant was collected for the additional centrifugation and the resulting pellet was dissolved in 2% SDS buffer for nuclear fraction. The supernatant was centrifuged at 165,000 × *g* for 60 min. The supernatant was prepared for cytosolic fraction, and the resulting pellet was dissolved in 2% SDS buffer as the ER and vesicle fraction. SH-SY5Y cells, HEK293T cells, ATF6α WT and ATF6α KO mouse embryonic fibroblasts (MEFs) were lysed in lysis buffer containing 1% Triton X-100 or 2% SDS buffer containing protease inhibitor and phosphatase inhibitor mixture. 20 or 30 μg of protein for each sample was separated by SDS-PAGE and electroblotted onto PDGF membrane (Immunopore). Immunoblotting analysis was carried out using an enhanced chemiluminescence Western blotting detection system kit (Amersham Biosciences). Rabbit anti-ATF6α polyclonal antibody was prepared as previously described (13). Mouse anti-BiP antibody was purchased from BD Biosciences (San Diego, CA). Rat anti-GRP94 antibody was purchased from Stressgen (Ann Arbor, MI). Rabbit anti-Derlin-3 antibody was purchased from Sigma-Aldrich. β-Actin antibody, anti-p38MAPK antibody, anti-phosho-p38MAPK (p-p38MAPK) antibody and anti-IRE1α antibody were obtained from Cell Signaling (Boston, MA). Rabbit anti-DAT antibody and mouse anti-tyrosine hydroxylase (TH) antibody were purchased from Millipore (Billerica, MA). Rabbit anti-ubiquitin antibody was purchased from DAKO (Glostrup, Denmark). Goat anti-PERK and rabbit anti-phospho-PERK antibody were obtained from Santa Cruz Biotechnology.

Immunohistochemistry—Mice were injected with pentobarbital and perfused transcardially with PBS, followed by 4% paraformaldehyde in PBS. Mice were decapitated, and their brains were removed and immersed in 4% paraformaldehyde in PBS for fixation. Serial coronal sections at 20-μm thickness were collected on slides. Deparaffinized sections were rinsed with PBS containing 0.1% Triton X-100 and then immersed in 0.3% H_2O_2 for 30 min. Sections were stained with primary antibodies against TH (mouse monoclonal; Millipore), BiP (IMGENEX, San Diego, CA) or ubiquitin (DAKO) or p-p38MAPK (Cell Signaling) in 10% normal serum overnight at 4 °C. After washing three times in PBST, the sections were stained with biotinylated secondary antibodies (Vector Laboratories, Burlingame, CA), using the standard avidin-biotin peroxidase method (Elite standard kit SK6100; Vector Laboratories, Burlingame, CA). SH-SY5Y cells, HEK293T cells and primary cultured dopaminergic neurons cultured in 4-well tissue culture chamber were fixed with 10% formaldehyde for 60 min on ice followed by acetone treatment for 5 min. They were then permeabilized with PBS containing 0.2% Triton X-100 for 10 min at room temperature and blocked with 10% goat serum for 30 min. They were then exposed to primary antibody overnight at 4 °C for indirect immunofluorescence. Anti-p38MAPK antibody and anti-p-p38MAPK were diluted 25-fold and 100-fold, respectively, with PBS containing 1% BSA before use. For immunofluorescence, primary antibodies were visualized by incubation for 2 h at room temperature with Alexa Fluor488- and Alexa Fluor546-conjugated secondary antibodies (Molecular Probes), followed by confocal laser scanning fluorescence microscopy using an LSM510 microscope(Carl Zeiss, Thornwood, NY).

TH-positive Cell and Ubiquitin-positive Inclusion Counting—Total numbers of TH-positive neurons in the substantia nigra pars compacta (SNc) and ubiquitin-positive inclusions in the striatum were determined using an unbiased optical fractionator method (Stereoinvestigator, MicroBrightField) as previously described with minor modification (4). Three independent sets of immunostained serial sections (sampled as every sixth coronal section throughout the entire range of SNc or the striatum) were analyzed for each animal. Total positive number for each sample was determined in triplicate by the Stereoinvestigator program to obtain averaged values. Location of SNc and the striatum was identified according to established anatomical landmarks (Paxinos mouse brain atlas).

Measurements of Striatal Catecholamines (HPLC)—Tissues dopamine and metabolites were measured according to previously published methods (4).

Plasmids, Cell Culture, Reagent, and Transfection—Various vectors, including pCMVfull-EGFP-ATF6α (also known as green fluorescent protein (GFP)-ATF6α fusion gene) (11), pGL3-GRP78 (−132)-Luc carrying the human BiP promoter, pGL3–5×UPRE-luc, pDNA3.1 (+)-N-terminal fragment of ATF6α (1–373) and a dominant-negative form of ATF6α (171–373) were prepared as previously (13, 14). Flag-p38MAPK was kindly provided by Dr. Katsuji Yoshioka (Kanazawa Univ.) ATF6α WT/KO primary cultured dopaminergic neurons were prepared as shown under "Primary culture." ATF6α WT/KO MEFs were obtained as previously described (7). SH-SY5Y cells were cultured in DMEM supplemented with 10% fetal bovine serum, NEAA (Invitrogen) at 37 °C in a humidified 5% CO_2/95% air atmosphere. HEK293T cells and ATF6α WT/KO MEFs were cultured in DMEM supplemented with 10% fetal bovine serum, 2 mM glutamine, and antibiotics (100 units/ml penicillin and 100 μg/ml streptomycin). Transfection was performed using Lipofectamine 2000 (Invitrogen, Carlsbad, CA) according to each manufacturer's protocol. 1-Methyl-4-phenylpyridinium iodide (MPP^+) was purchased from Sigma-Aldrich. SB203585 were purchased from Calbiochem (San Diego, CA). SHSY5Y cells and ATF6α WT/KO primary cultured dopaminergic neurons were treated with 1 mM MPP^+ for indicated times in the presence or absence of 5 μM SB203585. ATF6α WT/KO MEFs and HEK293T cells were plated in 6-well plates and treated with 50 μM hydroxyl peroxide (H_2O_2) (Nakalai Tesque, Kyoto) in the presence or absence of 5 μM SB203585.

Primary Culture—Mesencephalic and striatal cells were prepared from embryonic day 15 ATF6α WT/KO mice. Both the midbrain and the striatum were mechanically dissected in Neurobasal medium (Invitrogen). The tissues were dissociated with 0.25% trypsin at room temperature for 15 min. The cells were suspended in DMEM supplemented with 10% fetal bovine serum and NEAA and then collected by centrifugation (1000 × *g*, 3 min). The cells were resuspended in Neurobasal medium supplemented with B-27(minus Anti-Oxidants) (Invitrogen) and 0.5 mM glutamine at a concentration of 1million cells/ml, and plated at a density of 0.5 million cells per well into 24 well plate previously coated with poly-L-Lysin (Sigma-Aldrich). One week after plating, the cells were used for reporter assay or immunohistochemistry.

Reporter Assay—SH-SY5Y cells, HEK293T cells and ATF6α WT/KO primary cultured dopaminergic neurons were transiently transfected with pGL3–5×UPRE or pGL3-BiP (-132) along with pRL-SV40 (Promega, Madison, WI) using Lipofectamine 2000 (Invitrogen). After 48 h, the cells were treated with 1 mM MPP^+ for 24 h or 50 μM H_2O_2 for 1 h in the presence or absence of 5 μM SB203585. Luciferase expression was measured in triplicate using a dual luciferase reporter assay system (Promega) on Fluoroskan Ascent FL (Thermo, Waltham, MA). Relative activity was defined as the ratio firefly luciferase activity to *Renilla* luciferase activity to normalize for transfection efficiency.

Immunoprecipitation—After being washed with PBS, SH-SY5Y cells and HEK293T cells cultured in a 6-well plate dish were solubilized for 30 min on ice in 200 μl of RIPA buffer (50 mM Tris-HCl, 150 mM NaCl, 1 mM EDTA, 1% Triton X-100, 0.1% SDS, and 0.1% sodium deoxycholate) with a protease inhibitor mixture and a phosphatase inhibitor. Insoluble fraction was collected by centrifugation (1000 × *g*, 3 min), defined as nuclear fraction, and lysed in SDS lysis solution (50 mM Tris-HCl, 10 mM EDTA, 1% SDS) including phosphatase inhibitor. Soluble lysates were incubated overnight with ANTI-FLAG M2 Affinity gel (Sigma-Aldrich). Lysates from nuclear fraction were diluted to 10% by dilution buffer (50 mM Tris-HCl, 167 mM NaCl, 1.1% Triton X-100, and 0.11% sodium deoxycholate) including phosphatase inhibitor and then incubated for overnight by G-Sepharose bound to anti-phospho-p38MAPK antibody(Cell Signaling). Sepharose beads were collected by brief centrifugation and washed with TBS buffer (50 mM Tris-HCl, 150 mM NaCl, pH7.4) three times. Immunoprecipitated material was eluted by boiling for 3 min in 2× sample buffer (125 mM Tris-HCl, pH 6.8, 4% SDS, 20% glycerol, 0.004% BPB).

Chromatin Immunoprecipitation (ChIP) Assay—SH-SY5Y cells were grown to 80% confluence in 6-cm plates and then treated with 1 mM MPP^+ for 24 h and protein-DNA cross-linking was initiated by adding formaldehyde to the cell culture to a final concentration of 1% and stopped at 15 min by adding 1.5 M glycine to a final concentration of 0.15 M. The cells were lysed in RIPA buffer including a protease inhibitor mixture and a phosphatase inhibitor. Insoluble fraction was collected by centrifugation (1000 × *g*, 3 min), defined as nuclear fraction, lysed in SDS lysis solution (50 mM Tris-HCl, 10 mM EDTA, 1% SDS) including phosphatase inhibitor and sonicated for 25 min using Bioruptor (UCD-200TM, COSMO BIO) (Sonication pulse was performed by power high, ON 30 s, OFF 60 s). Diluted to 10% by ChIP dilution buffer (50 mM Tris-HCl, 167 mM NaCl, 1.1% Triton X-100, and 0.11% sodium deoxycholate) including phosphatase inhibitor, lysates were incubated for overnight by G-Sepharose bound to anti-phospho-p38MAPK antibody. Sepharose beads were collected by brief centrifugation, washed with RIPA buffer three times and suspended with ChIP direct elution buffer (10 mM Tris-HCl, 300 mM NaCl, 5 mM EDTA, 0.5% SDS). Formaldehyde-induced cross linking was reversed (for overnight at 65 °C) and the DNA was purified by phenol-chloroform extraction and ethanol precipitation. Purified DNA was subjected to quantitative PCR by LightCycler 480 program.

Statistical Analysis—All values are presented as the mean ± S.D. Results were tested for significant differences using one-way ANOVA with the posthoc test or Student's *t* test. $p < 0.05$ was considered to represent significant difference. In figures, a single asterisk (*) indicates $p < 0.05$, and a double asterisk (**) indicates $p < 0.01$.

RESULTS

ATF6α Controls the Levels of ER Chaperones and ERAD Component in the Dopaminergic Neuron System in Vivo—To explore the physiological function of ATF6α *in vivo*, we first investigated where in the central nervous system ATF6α is

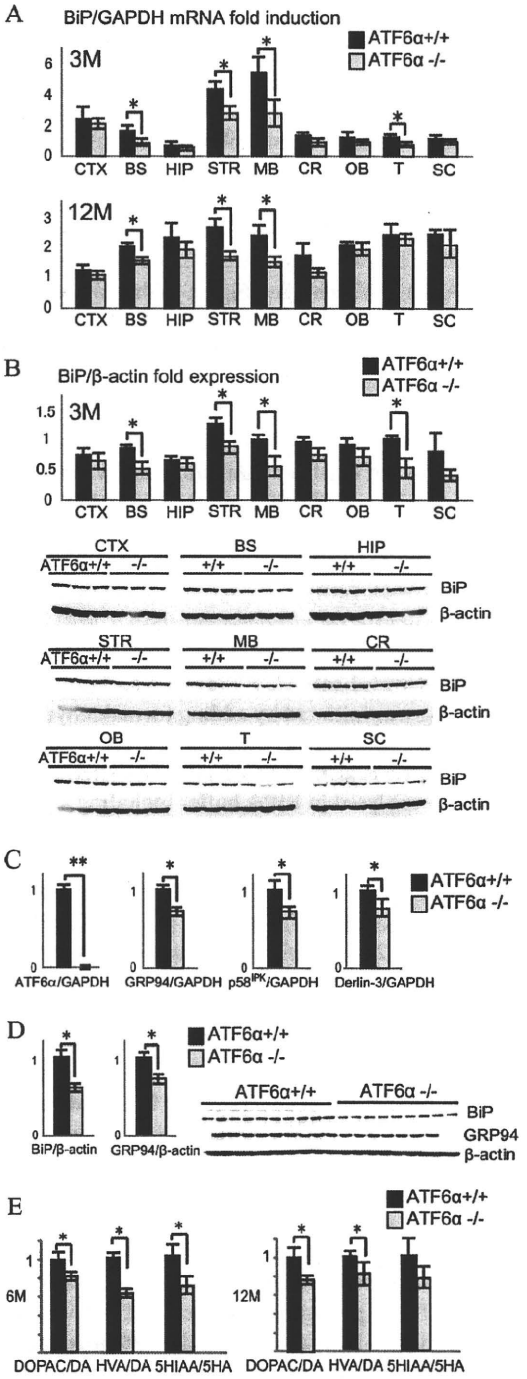

FIGURE 1. **ATF6α controls the levels of ER chaperones and ERAD component in the dopaminergic neuron system under physiological conditions *in vivo*.** *A*, ATF6α controls the mRNA levels of BiP in the brainstem, the midbrain and the striatum in mice brain *in vivo*. Total RNA was isolated from various sections of brain of 3 and 12-month-aged male ATF6α KO(−/−) mice and ATF6α WT(+/+) littermates and analyzed by quantitative real-time RT-PCR for detecting the level of BiP mRNA. ($n = 5$ for each group). Fold induction of mRNA level is defined relative to GAPDH mRNA level. Abbreviation: *CTX*, cerebral cortex; *BS*, brainstem; *HIP*, hippocampus; *STR*, striatum; *MB*, midbrain; *CR*, cerebellum; *OB*, olfactory bulb; *T*, thalamus; *SC*, spinal cord; 3 M, 3 months aged group; 12 M, 12-month-aged group. The *asterisk* indicates statistical significance (*, $p < 0.05$; **, $p < 0.01$). Each bar denotes the mean ± S.D. *B*, ATF6α controls the protein levels of BiP in the brainstem, the midbrain and the striatum in mice brain *in vivo*. The tissue lysates of 3-month-aged ATF6α KO mice and ATF6α WT littermate were subjected to Western blot analysis for detection of BiP and β-actin ($n = 5$). Each protein level was quantified using optical density and estimated relative to β-actin protein level. *C*, ATF6α controls the levels of GRP94, p58^{IPK}, and Derlin-3 in the midbrain *in vivo*. Quantitative real-time RT-PCR was performed from the midbrain samples of 12-month-aged ATF6α KO mice and ATF6α WT littermates using ATF6α, GRP94, p58^{IPK}, and Derlin-3 primers ($n = 5$ for each group). *D*, ATF6α controls the protein levels of BiP and GRP94 in the striatum *in vivo*. ($n = 7–10$). *E*, metabolisms of dopamine and serotonin were decreased in ATF6α KO mice as compared with ATF6α WT mice. Metabolisms of dopamine and serotonin were defined as the relative ratio of DOPAC or HVA to dopamine and 5HIAA to 5HA, respectively. The striatal levels of dopamine, serotonin, and their metabolites were measured by HPLC ($n = 8–10$ for each group). Abbreviations: *DA*, dopamine; *DOPAC*, 3,4-dihydroxyphenylacetic acid; *HVA*, homovanillic acid; *5HIAA*, 5-hydroxyindole acetic acid; *5HA*, 5-hydroxytryptamine; 6 M, 6-month-aged group; 12 M, 12-month-aged group.

activated under normal physiological conditions by using ATF6α WT or KO mice. Results of quantitative RT-PCR analysis demonstrated that mRNA level of the ER chaperone BiP was significantly lower in the brainstem, the midbrain and the striatum of ATF6α KO mice than those of ATF6α WT mice (Fig. 1*A*). Accordingly, the protein levels of BiP were also significantly lower in the brainstem, the midbrain and the striatum of ATF6α KO mice than those of ATF6α WT mice (Fig. 1*B*). Other ER stress sensor, IRE1α, sXBP1, and phosphorylated PERK (p-PERK, indicative of the activation status of another ER stress sensor molecule) are not different in various brain regions of ATF6α KO mice (supplemental Fig. S1*A*). The mRNA levels of other ER chaperone GRP94, cochaperone p58^{IPK}, and ERAD component, Derlin-3, in the midbrain were also significantly decreased in ATF6α KO mice when compared with age-matched ATF6α WT mice (Fig. 1*C*). The protein levels of GRP94 in the striatum were significantly decreased in ATF6α KO mice (Fig. 1*D*). HPLC analysis of the striatum demonstrated that the metabolisms of dopamine and serotonin were slightly but significantly decreased in ATF6α KO mice as compared with WT mice (Fig. 1*E*). Decreased protein levels were not general feature of ATF6α KO mice because the levels of some proteins involved in synaptic secretion or vesicular transport remained unchanged or rather increased in ATF6α KO mice as compared with WT mice (supplemental Fig. S1*B*). Importantly, tyrosine hydroxylase (TH) immunostaining of the midbrain revealed that there was no abnormality in the number and morphology of TH positive neurons in ATF6α KO mice when compared with WT littermates (supplemental Fig. S1, *C* and *D*). TH and DAT protein levels in the striatum of ATF6α KO mice were similar to those of WT littermates (supplemental Fig. S1*E*). Therefore, although ATF6α is not essential for the development and the survival of dopaminergic neurons, ATF6α up-regulates ER chaperones and ERAD component constitutively in dopaminergic neurons; dopaminergic neurons may experience ER stress under normal physiological conditions.

MPTP Up-regulates the Levels of ER Chaperones and ERAD Component by Activating ATF6α and Induces the Phosphorylation of p38MAPK in the Dopaminergic Neurons in Vivo—To investigate whether ATF6α plays an important role in dopaminergic cell death of neurotoxin-based PD models, we analyzed dopaminergic neurons of mice treated with MPTP. MPTP was intraperitoneally administered into 6-month-old